Electronic Supplementary Material (ESI) for Journal of Materials Chemistry C.

Supporting Information

Dual Emission and Multi-Stimuli-Response in Iridium(III) Complexes with Aggregation-Induced Enhanced Emission: Application to Quantitative CO_2 Detection

Clàudia Climent[a†], Parvej Alam[b†], Sheik Saleem Pasha[b], Gurpreet Kaur[c], Angshuman Roy Choudhury[c], Inamur Rahaman Laskar[b,*], Pere Alemany[a,*], David Casanova[d,e,*]

[a]Departament de Ciència de Materials i Química Física and Institut de Química Teòrica i Computacional (IQTCUB), Universitat de Barcelona, Martí i Franquès 1-11, Barcelona 08028, Spain.

[b]Department of Chemistry, Birla Institute of Technology and Science, Pilani Campus, Pilani, Rajasthan, India.

[c]Department of Chemical Sciences, Indian Institute of Science Education and Research (IISER), Mohali, Sector 81, S. A. S. Nagar, Manauli PO, Mohali, Punjab, 140306, India.

[d]Kimika Facultatea, Euskal Herriko Unibertsitatea (UPV/EHU), Donostia International Physics Center, Paseo Manuel de Lardizabal, 4, Donostia 20018, Spain.

[e]IKERBASQUE, Basque Foundation for Science, Bilbao 48013, Spain.

[†]Both authors contributted equally to this work, C.C with the computational part and P.A with the experimental part.

TABLE OF CONTENTS

Section 1. Experimental Characterization

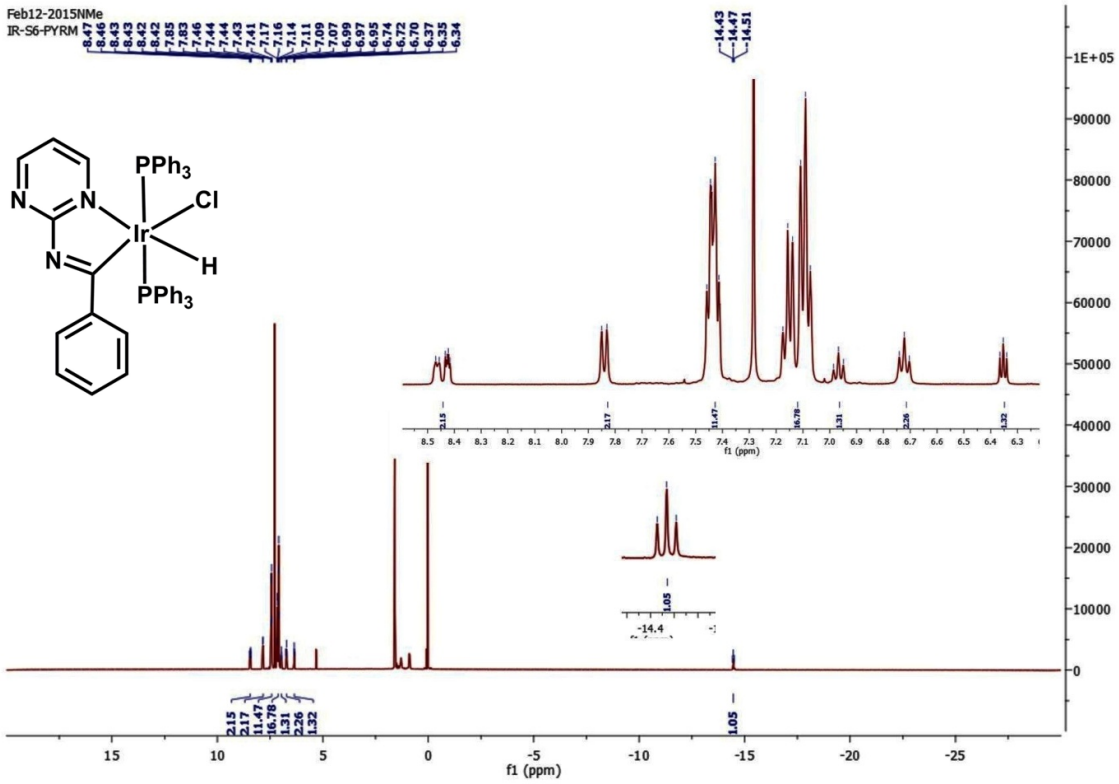

(a)

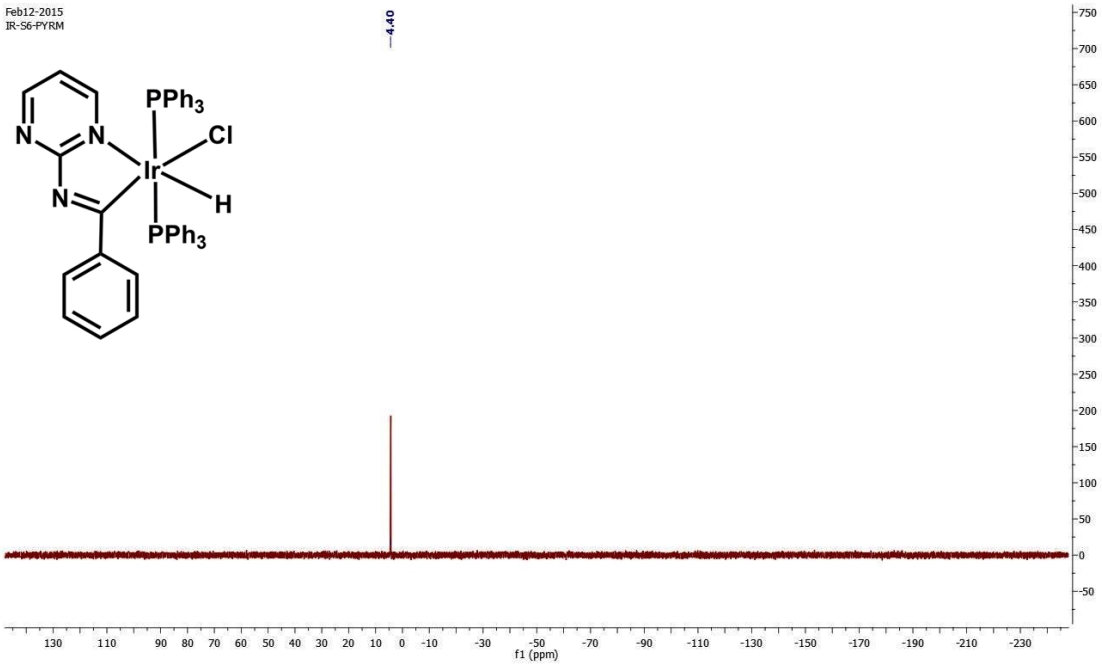

(b)

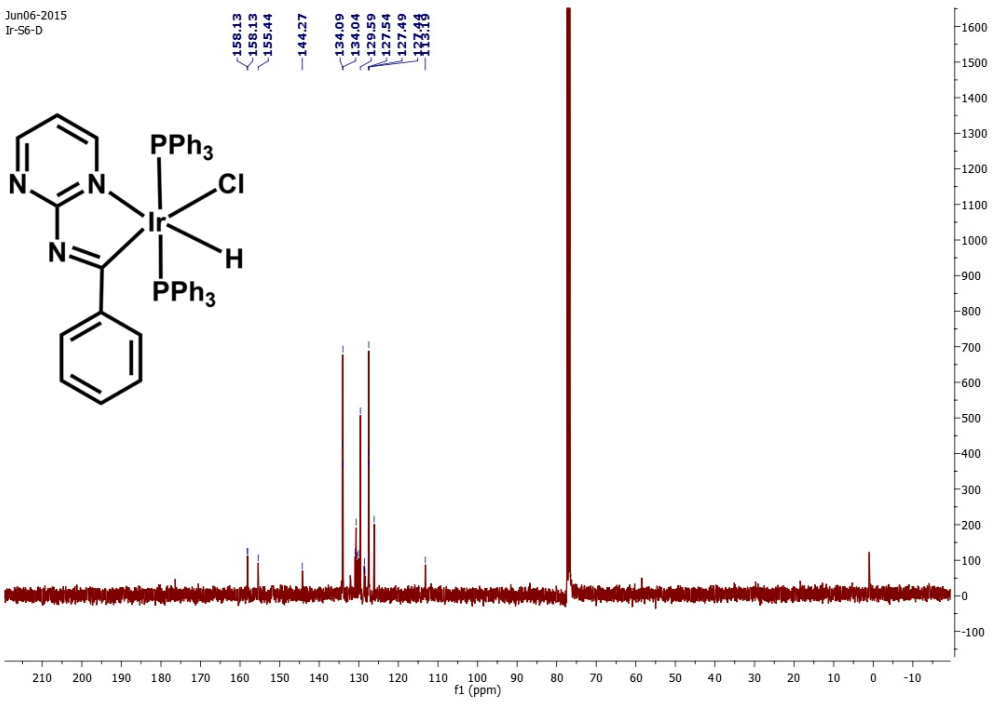

(c)

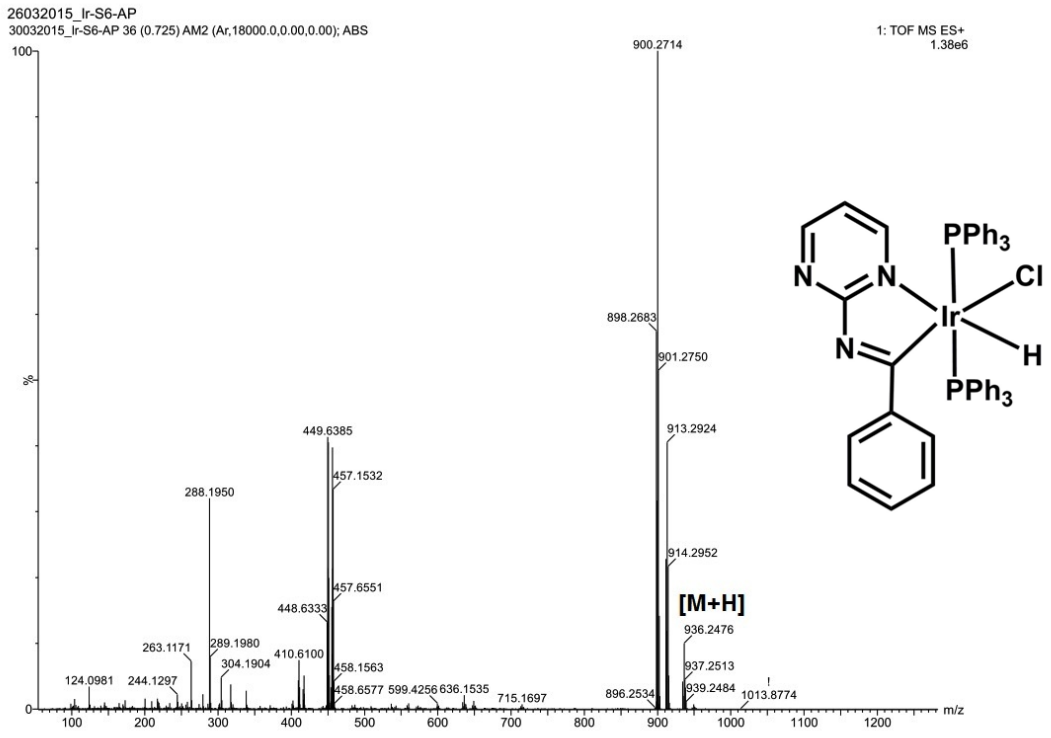

(d)

Figure S1. (^{1}H, ^{31}P and ^{13}C) NMR spectra and HRMS (a, b, c and d), respectively for **1.**

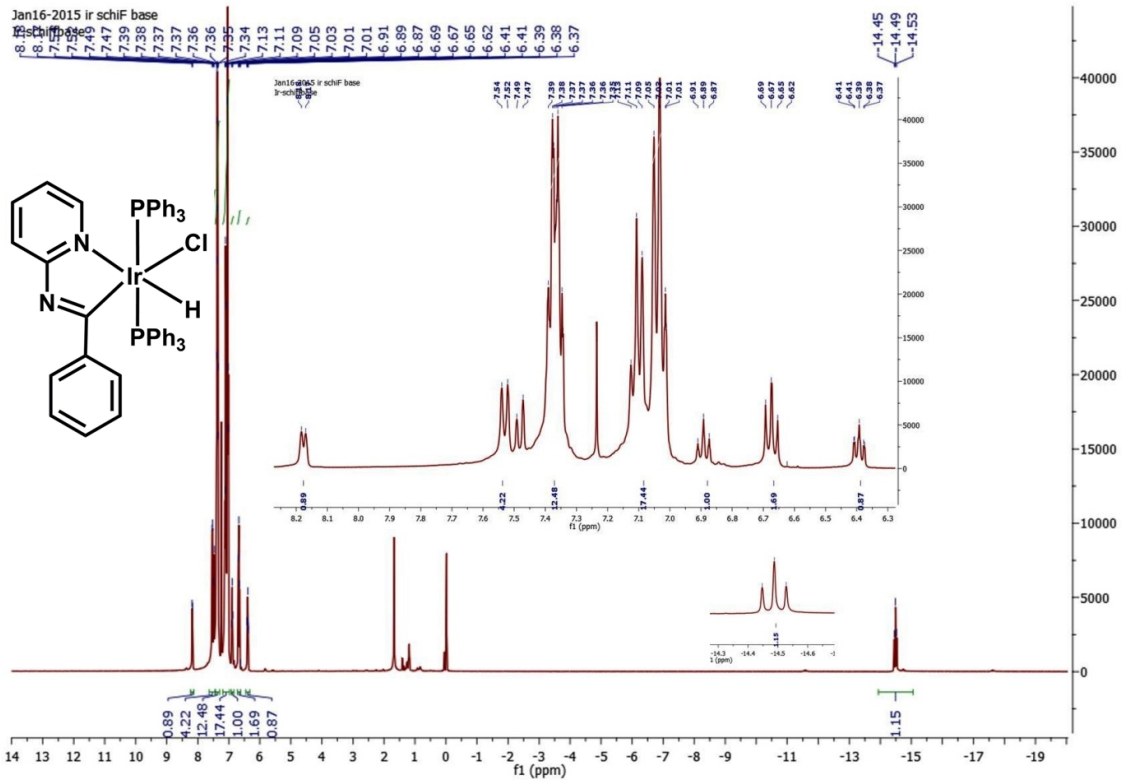
Jan16-2015 ir schiF base
PPh3
Cl
Ir
N
N
H
PPh3
f1 (ppm)

(a)

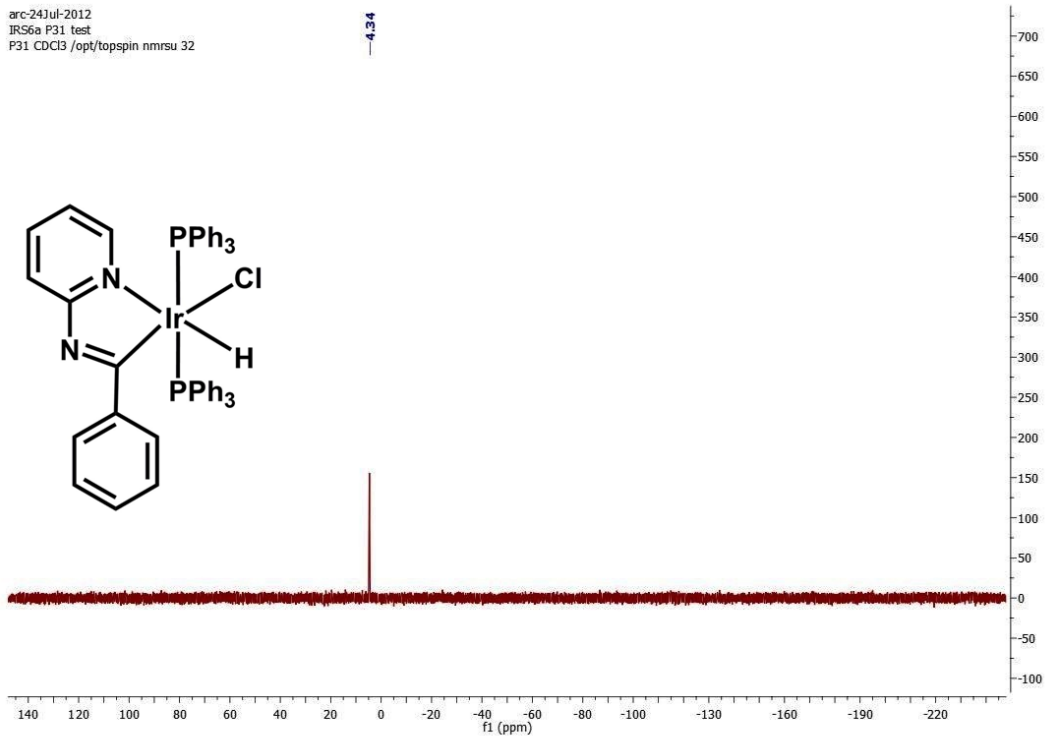
arc-24Jul-2012
IRS6a P31 test
P31 CDCl3 /opt/topspin nmrsu 32
4.34
PPh3
Cl
Ir
N
N
H
PPh3
f1 (ppm)

(b)

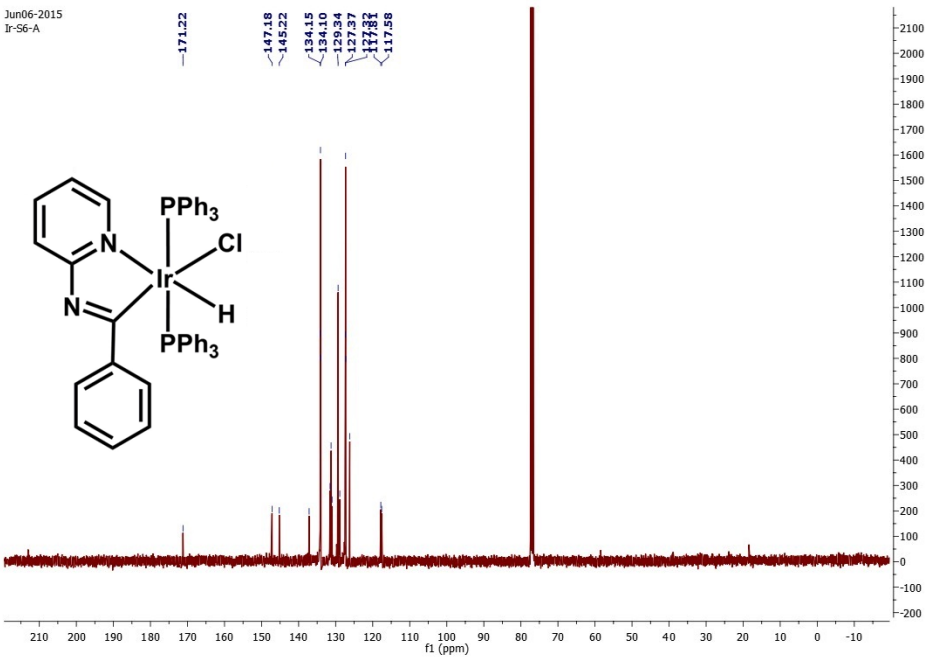

(c)

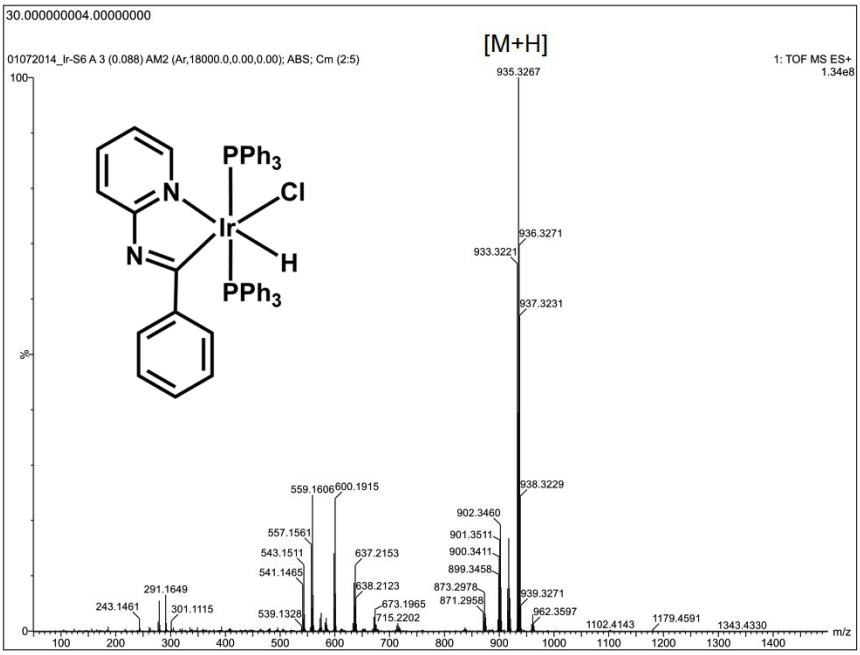

(d)

Figure S2. (^{1}H, ^{31}P and ^{13}C) NMR spectra and HRMS (a, b, c and d), respectively for **2**.

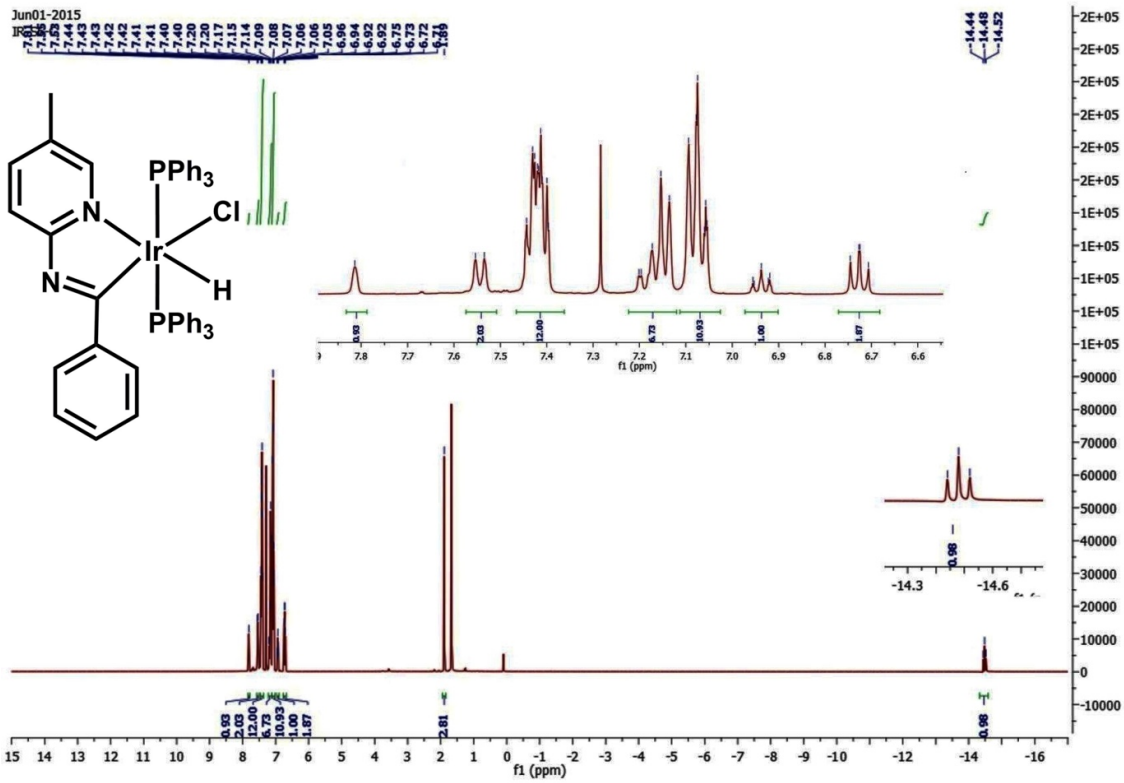
Jun01-2015
PPh3
Cl
Ir
N
N
H
PPh3
f1 (ppm)

(a)

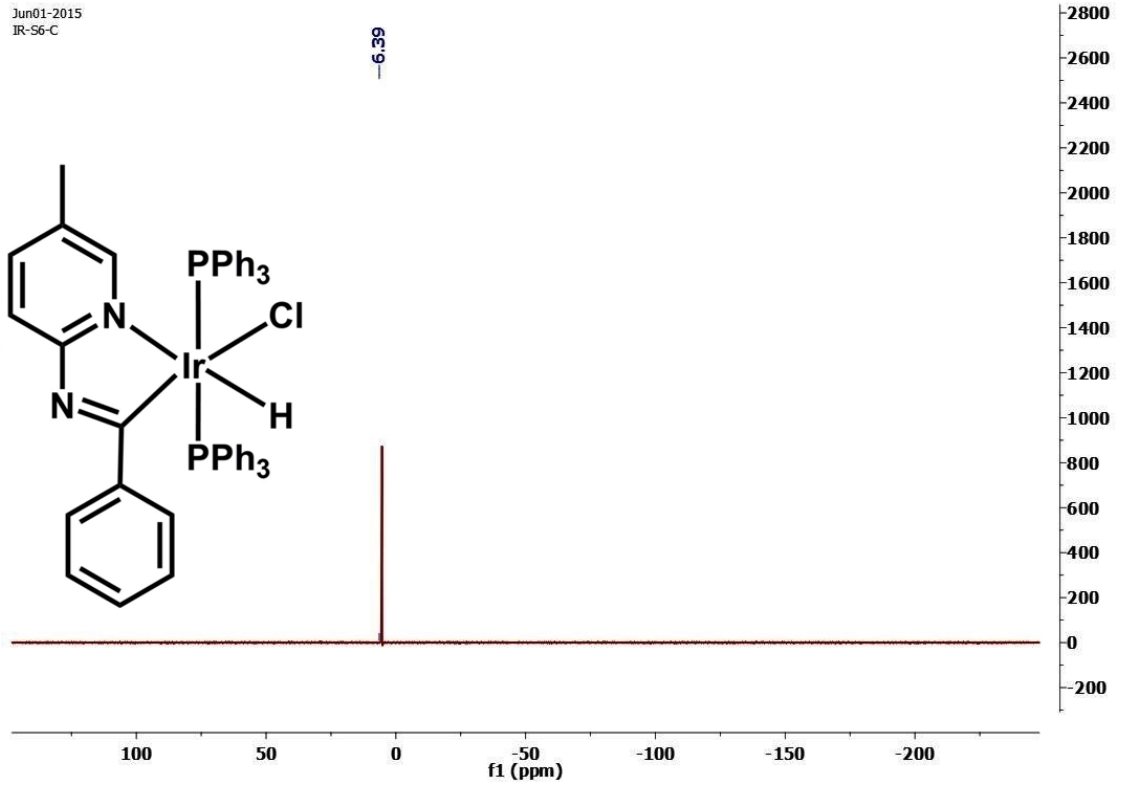
Jun01-2015
IR-S6-C
-6.39
PPh3
Cl
Ir
N
N
H
PPh3
f1 (ppm)

(b)

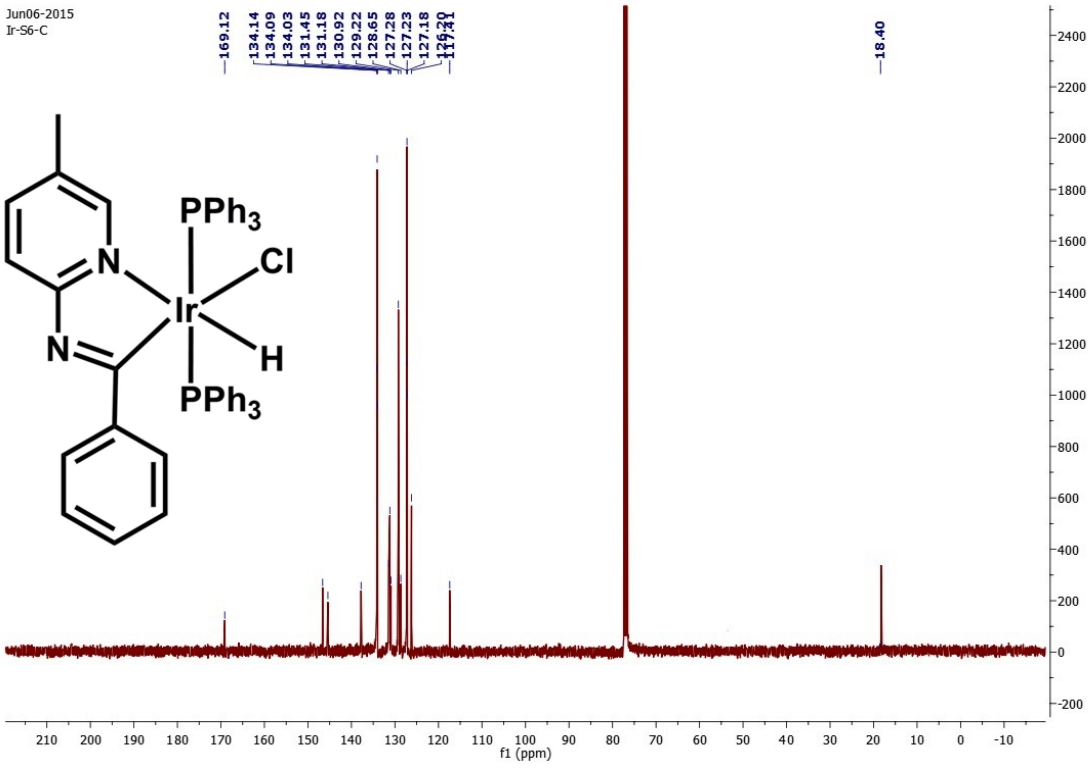

(c)

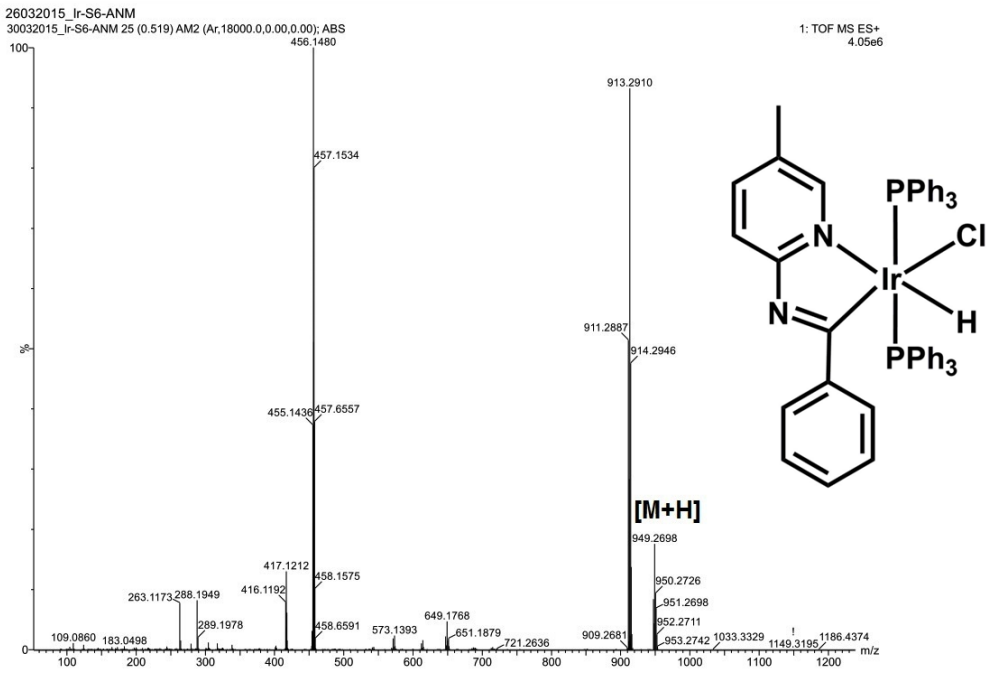

(d)

Figure S3. (^{1}H, ^{31}P and ^{13}C) NMR spectra and HRMS (a, b, c and d), respectively for **3**.

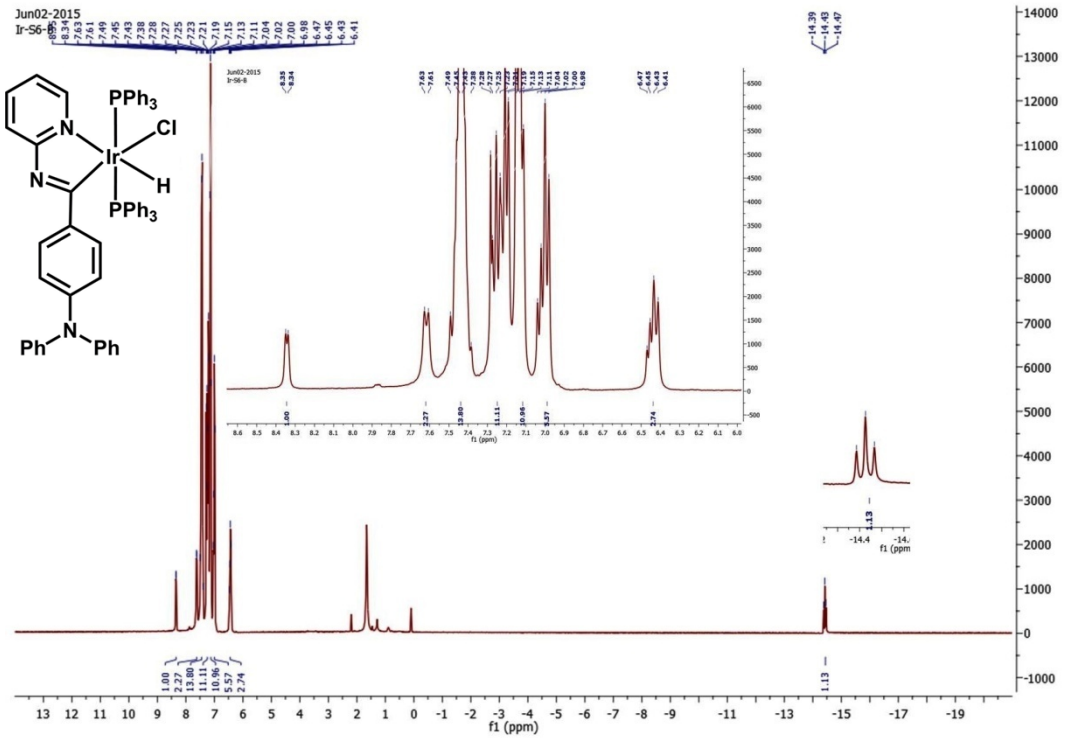
Jun02-2015
Ir-S6-B
PPh3
Cl
Ir
H
PPh3
N
N
Ph
N
Ph
f1 (ppm)

(a)

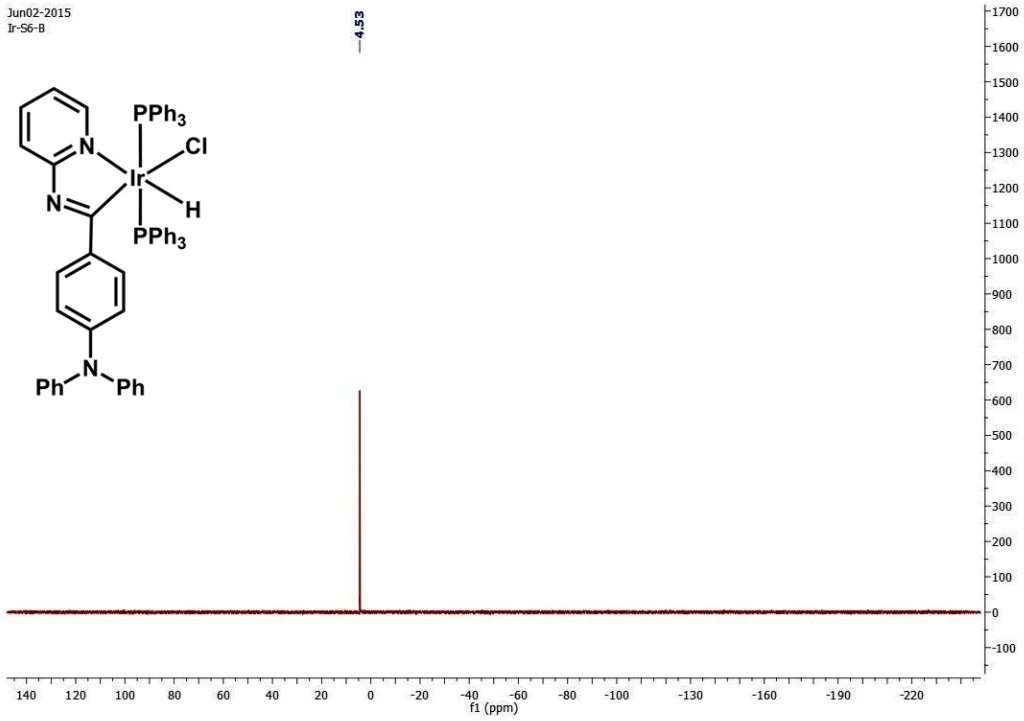
Jun02-2015
Ir-S6-B
-4.53
PPh3
Cl
Ir
H
PPh3
N
N
Ph
N
Ph
f1 (ppm)

(b)

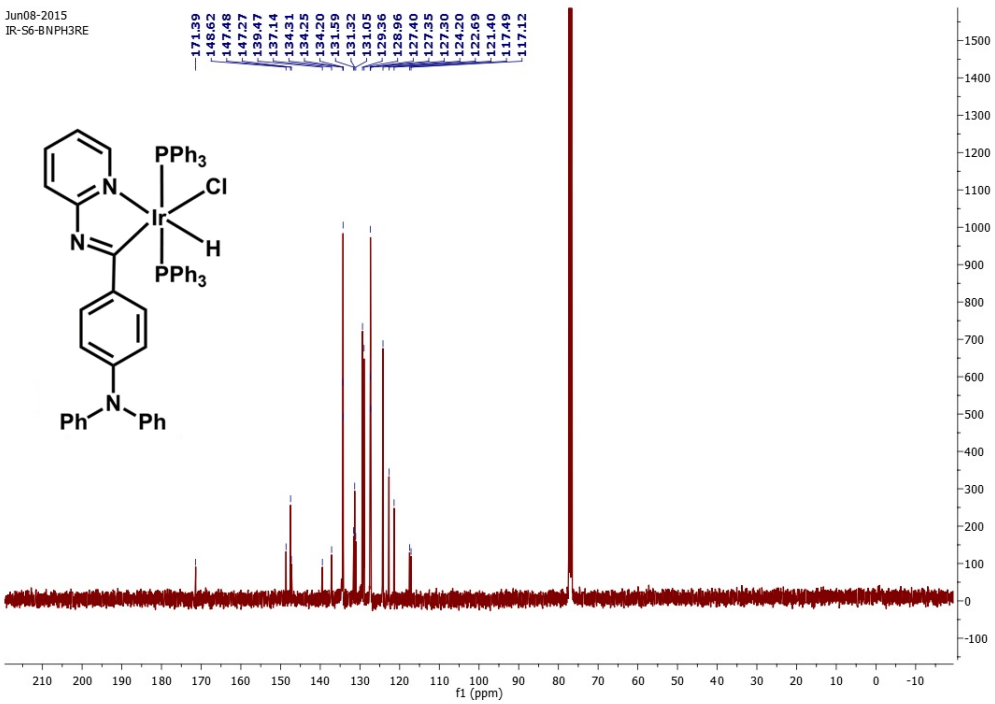

(c)

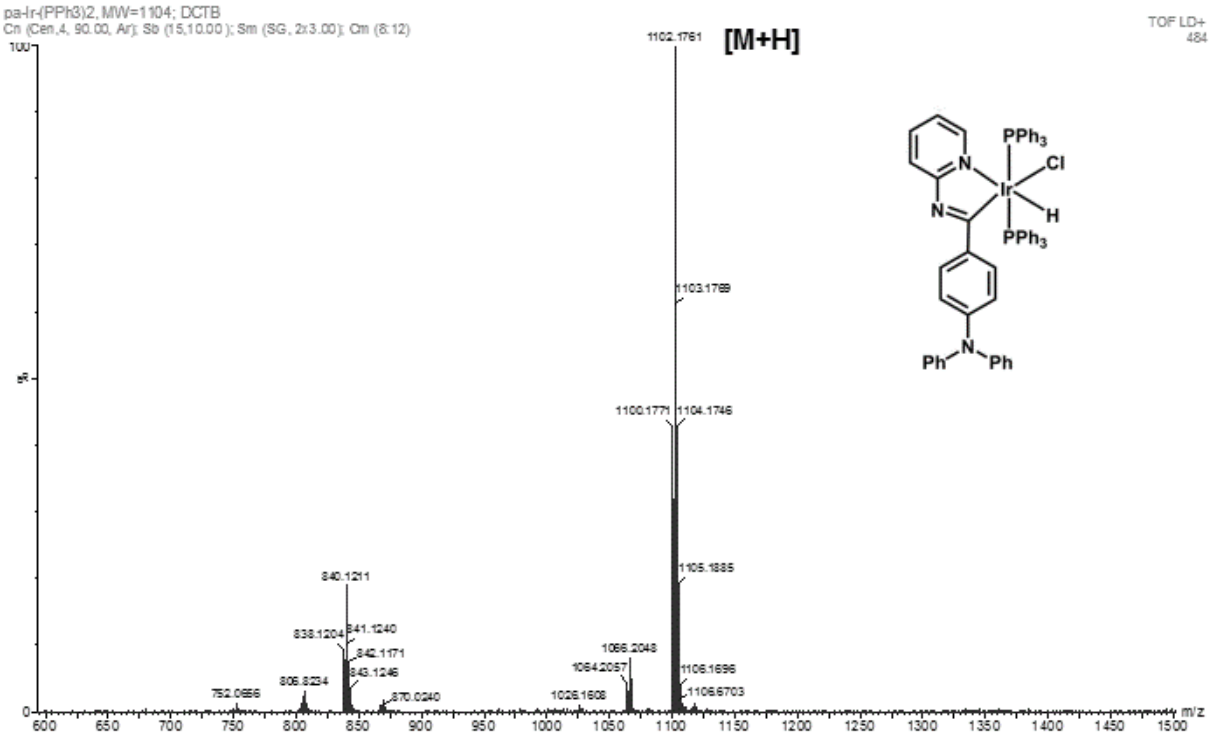

(d)

Figure S4. (^{1}H, ^{31}P and ^{13}C) NMR spectra and HRMS (a, b, c and d), respectively for **4**.

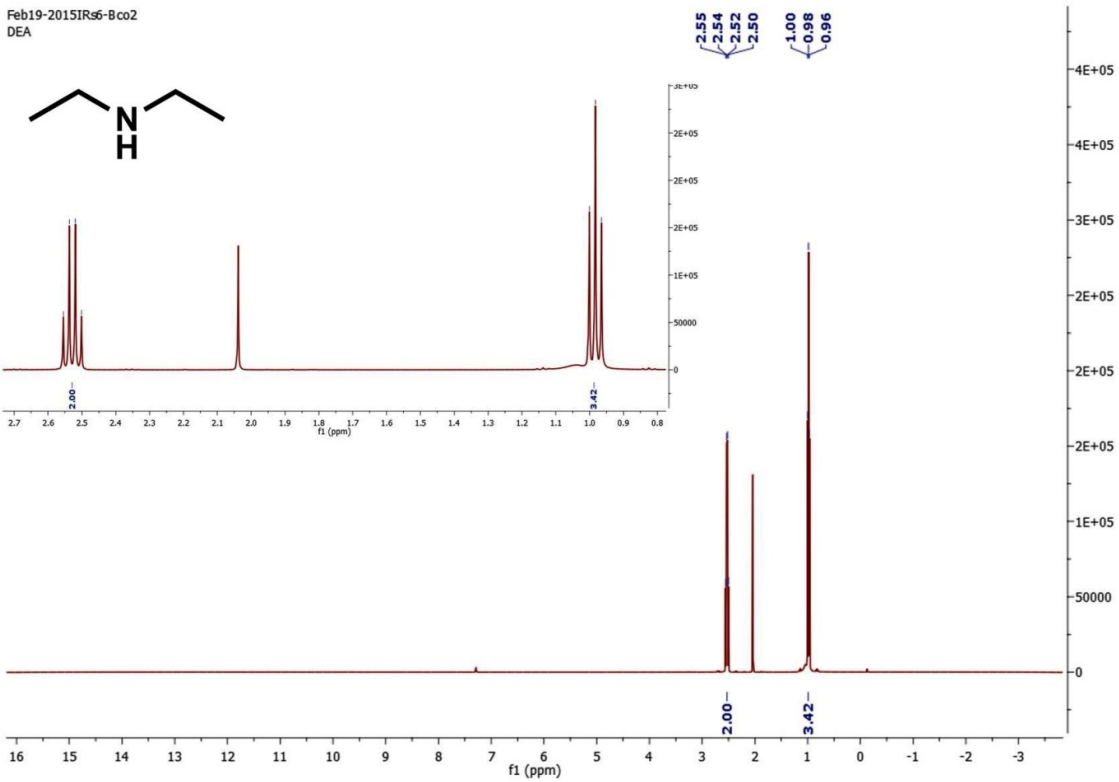

(a)

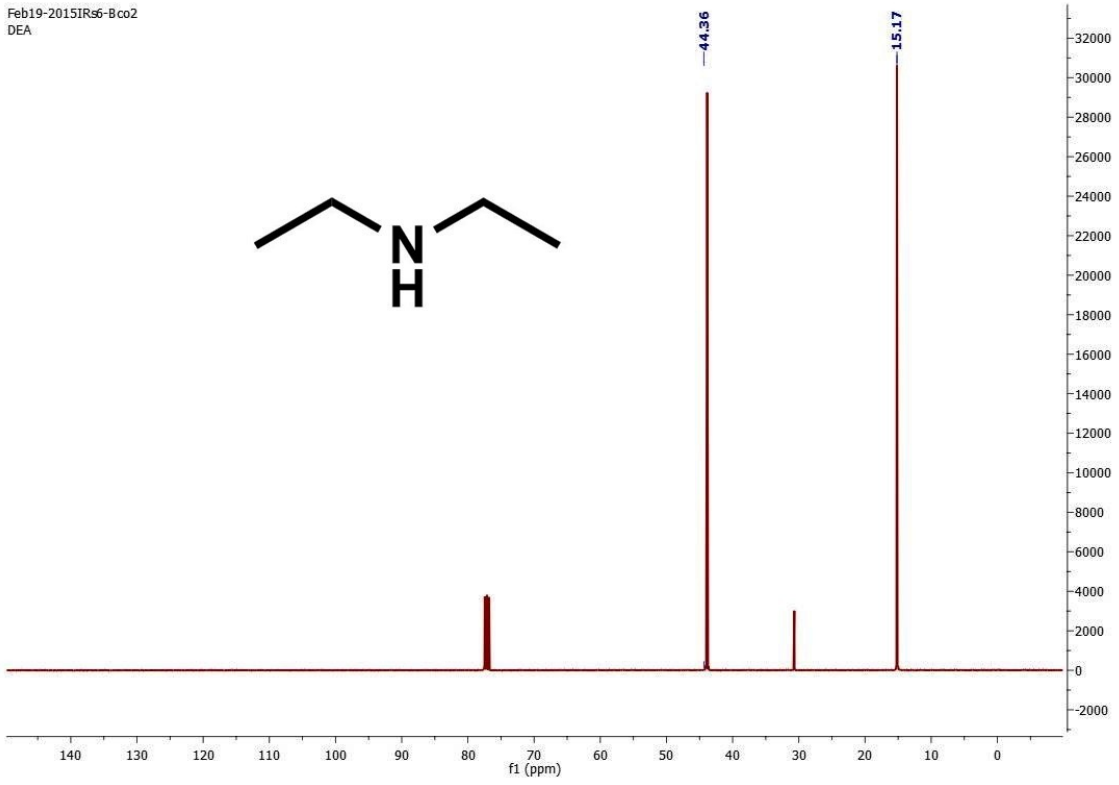

(b)

Figure S5. (^{1}H and ^{13}C) NMR spectra (a and b), respectively for **DEA**.

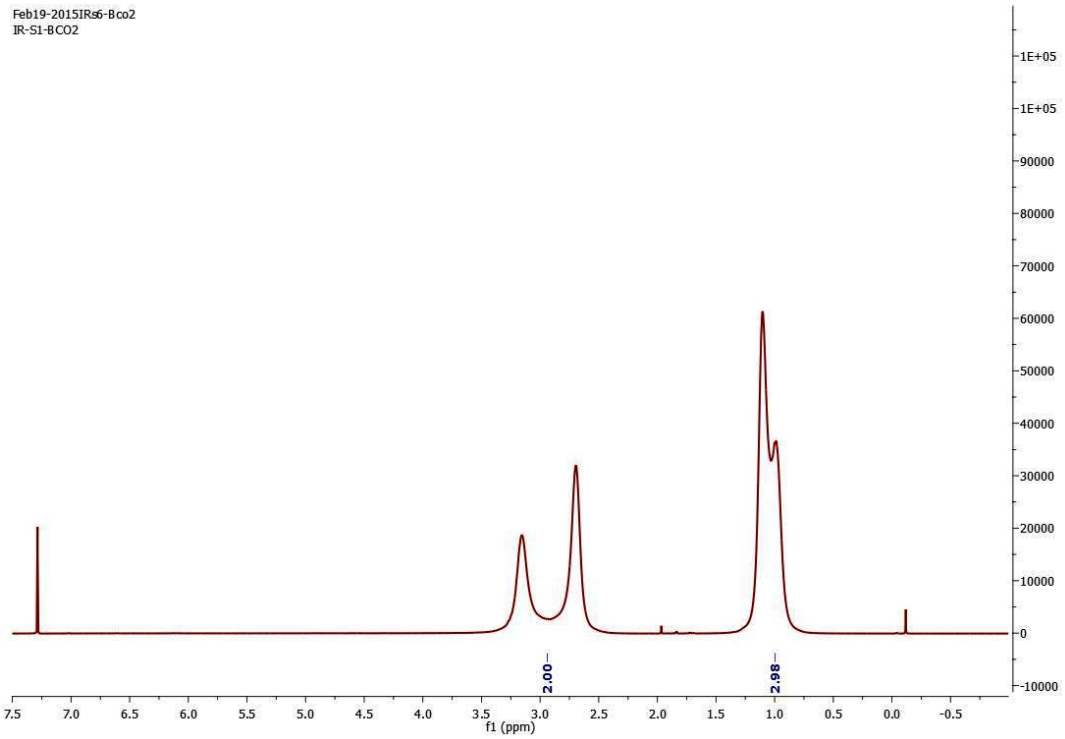

(a)

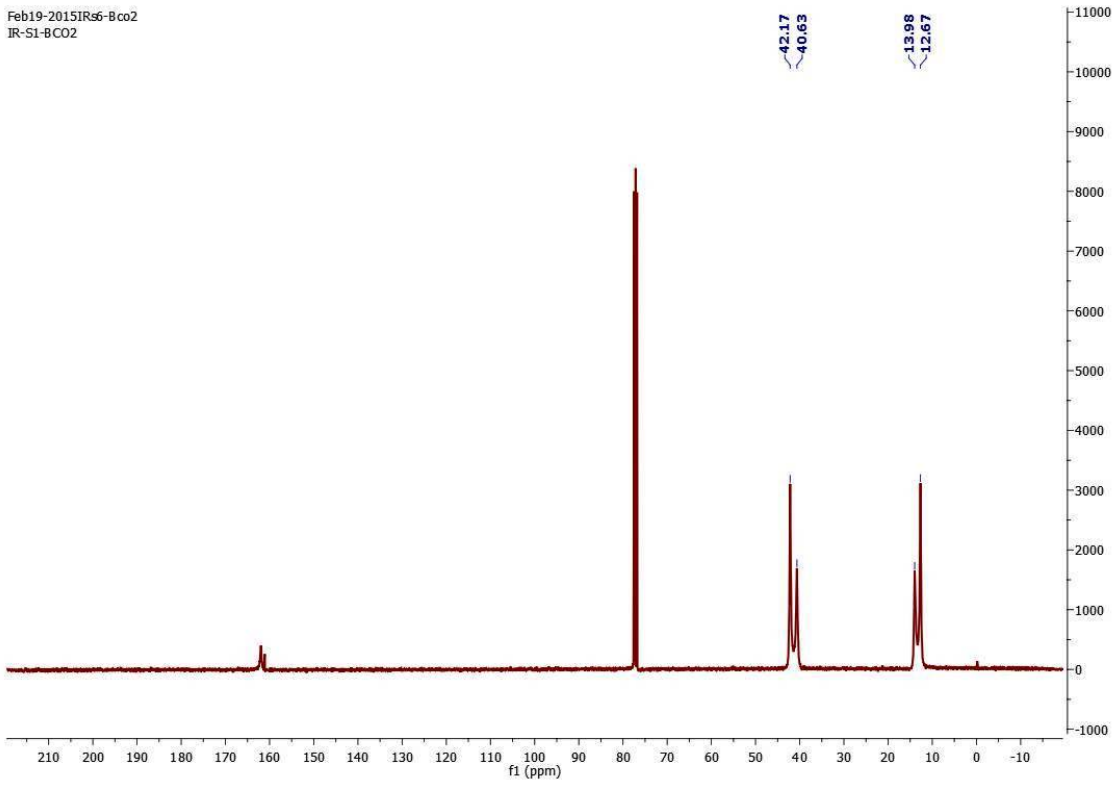

(b)

Figure S6. (^{1}H and ^{13}C) NMR spectra (a and b), respectively for **DEA+CIL**.

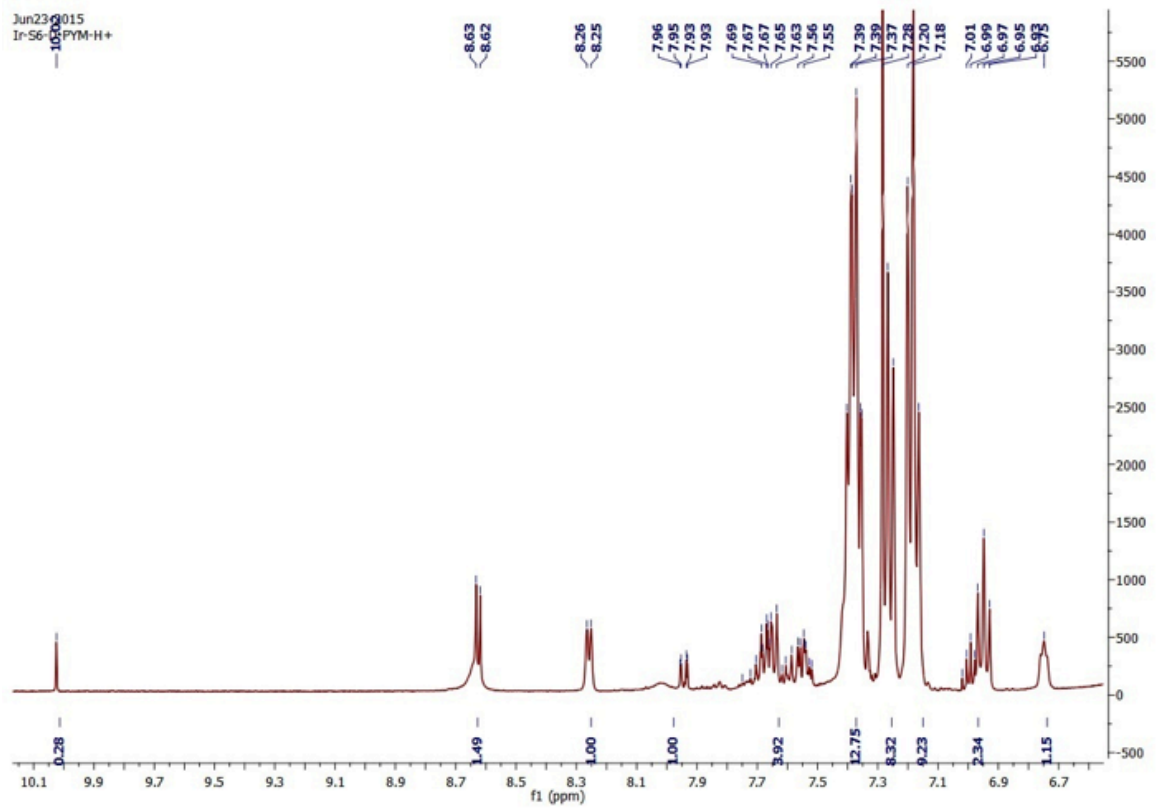

Figure S7. ^{1}H NMR spectra for **1+TFA**.

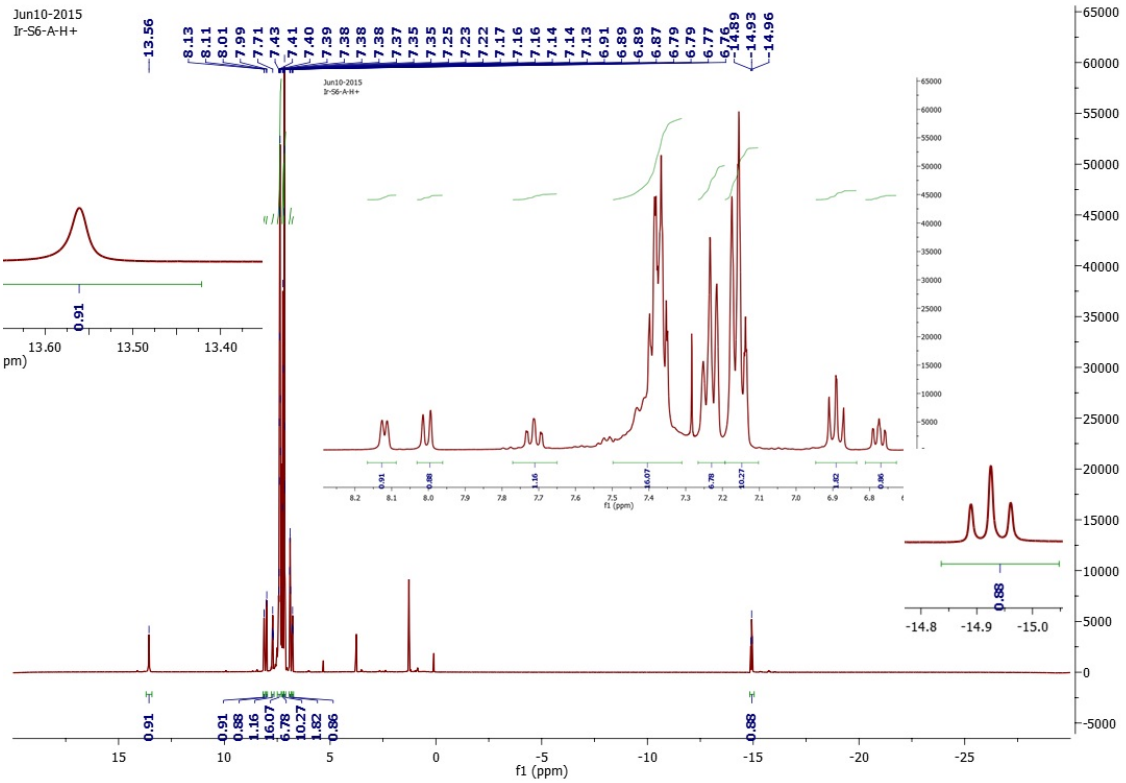

Figure S8. ^{1}H NMR spectra for **2+TFA**.

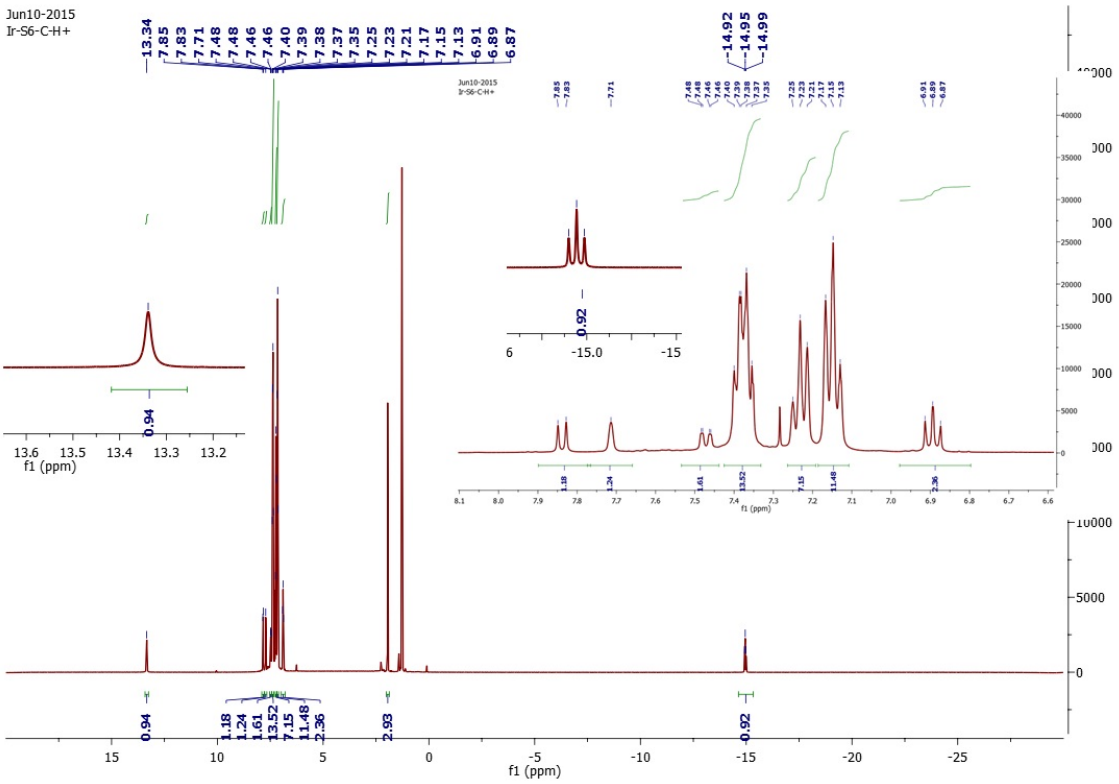

Figure S9. ^{1}H NMR spectra for **3+TFA**.

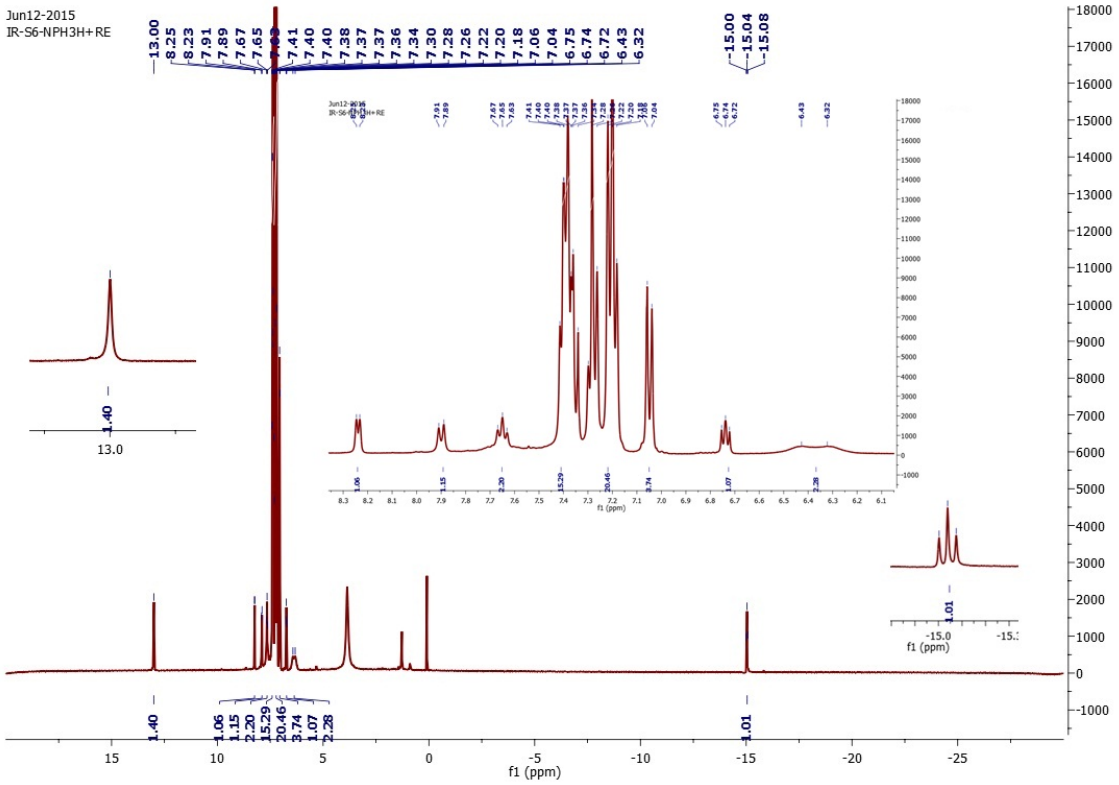

Figure S10. ^{1}H NMR spectra for **4+TFA**.

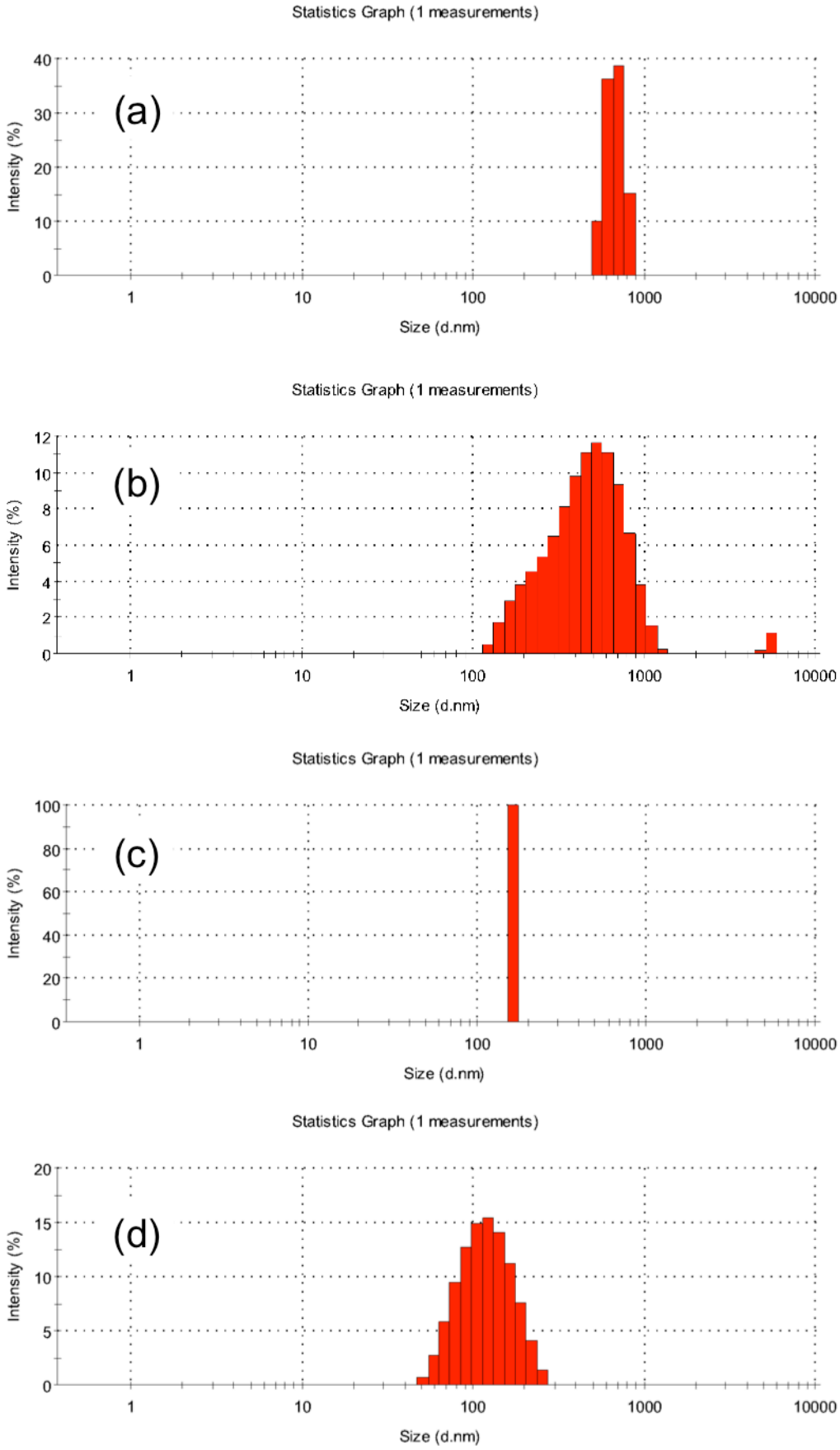

Figure S11. Particle size distribution of nano-aggregates of complexes **1-4** (a-d) in a THF/water mixture with a 90% of water fraction.

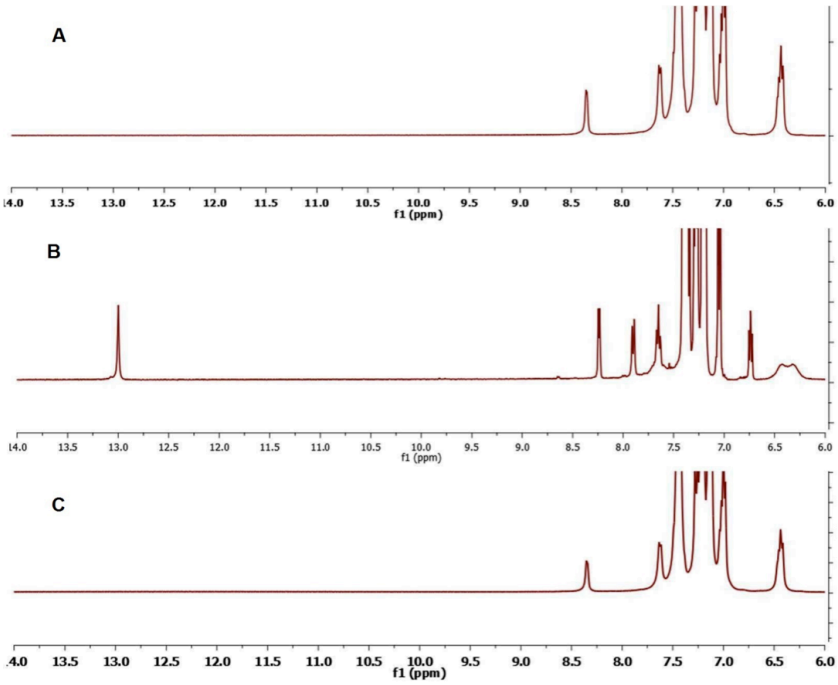

Figure S12. ^{1}H NMR spectra of **4** in $CDCl_3$ containing (A) 0 μL of trifluoroacetic acid (TFA) (B) 100 μL of TFA and (C) by addition of 250 μL of triethylamine (Et_3N) to (B).

Section 2. Absorption and Emission Spectroscopy

Emission color calculation

From the experimental emission spectra, the perceived colors by the human eye may be estimated following a very simple procedure using the standard CIE (2º) 1931 color space, which allows calculating the xy chromaticity coordinates [1]. The overlap between the emission spectra, ε(λ), and the color matching function, $\bar{x}(\lambda)$ in the visible range yields the X tristimulus value (equation 1). For the numerical integration, a 1 nm increment is sufficient to attain accurate results. The Y and Z tristimulus values may be calculated analogously with the corresponding $\bar{y}(\lambda)$ and $\bar{z}(\lambda)$ color matching functions (CMFs). These CMFs describe the observer in a given color space, characterizing its chromatic response. Their values may be found tabulated in the literature [2].

$$X = \int_{visible} \bar{x}(\lambda)\varepsilon(\lambda)d\lambda \tag{1}$$

Finally, the x and y chromaticity coordinates are calculated as:

$$x = \frac{X}{X+Y+Z} \qquad y = \frac{Y}{X+Y+Z} \tag{2}$$

References

[1] Schanda, J.; Colourimetry: Understanding the CIE System, Wiley, Hoboken, New Jersey, 2007
[2] http://cvrl.ioo.ucl.ac.uk/cmfs.htm

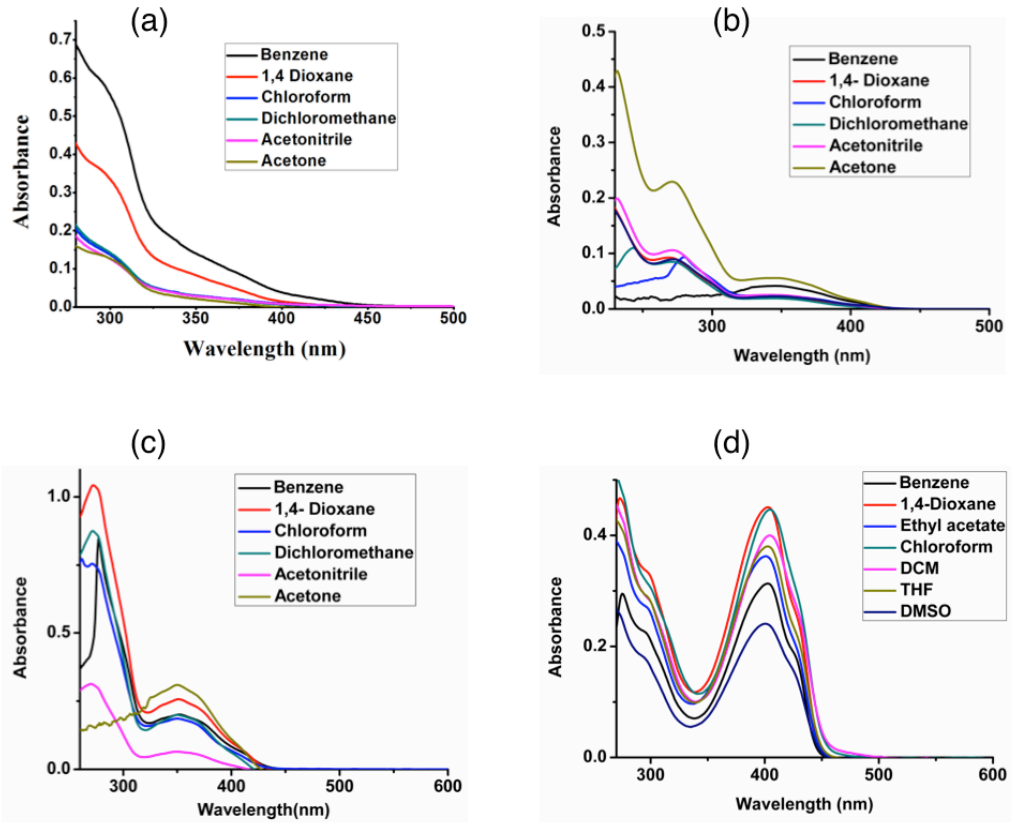

Figure S13. Absorption spectra of **1-4** (a-d) with varying solvent polarity.

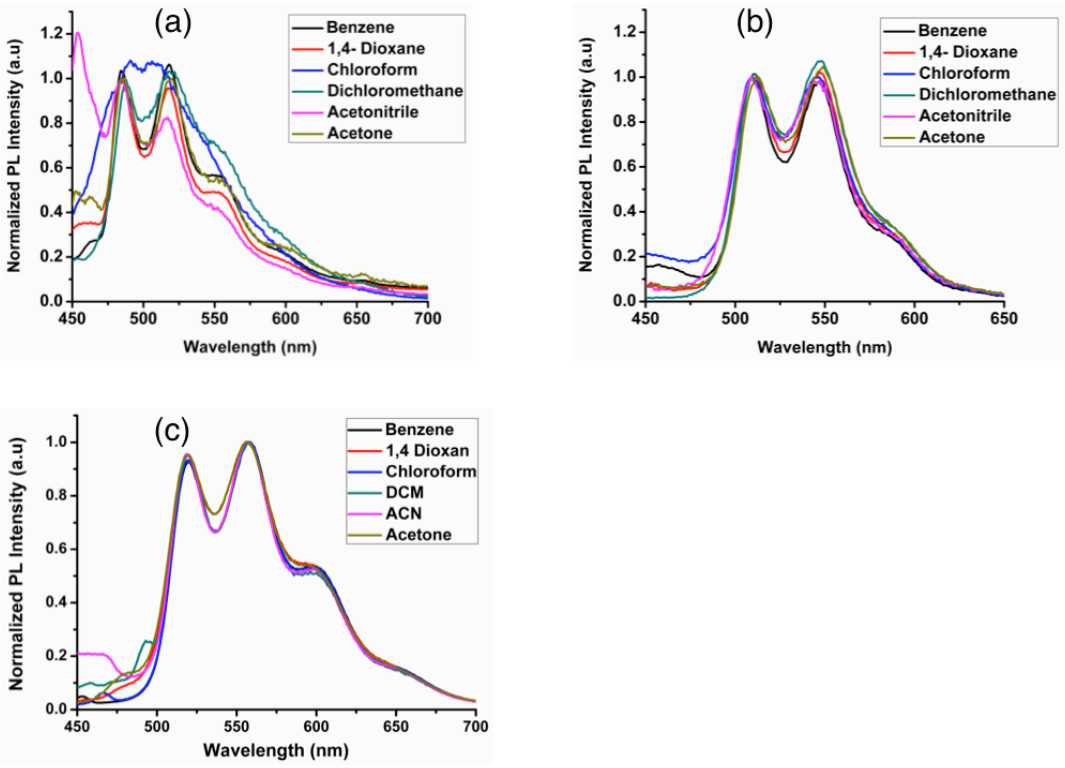

Figure S14. Emission spectra of **1-3** (a-c) with varying solvent polarity.

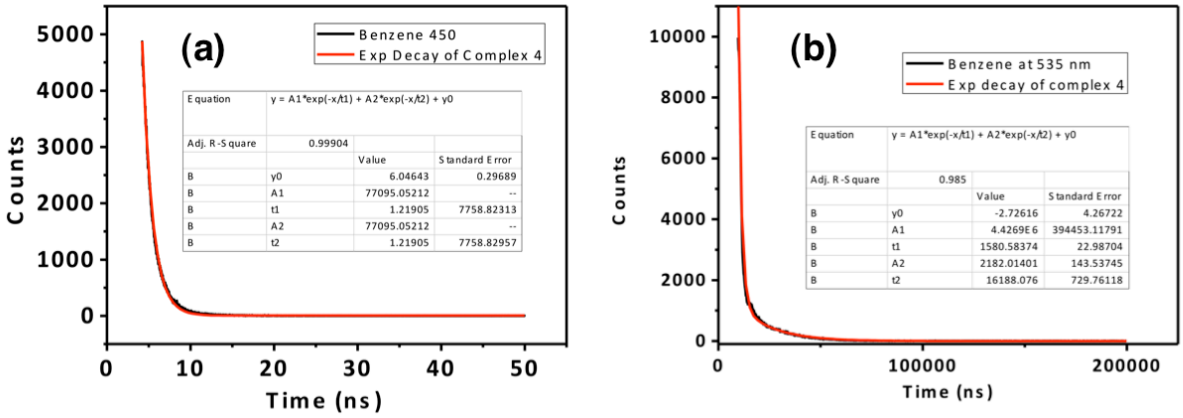

Figure S15. Emission decay profiles of **4** in benzene at different emission maxima (a) at 450 nm and (b) at 535 nm.

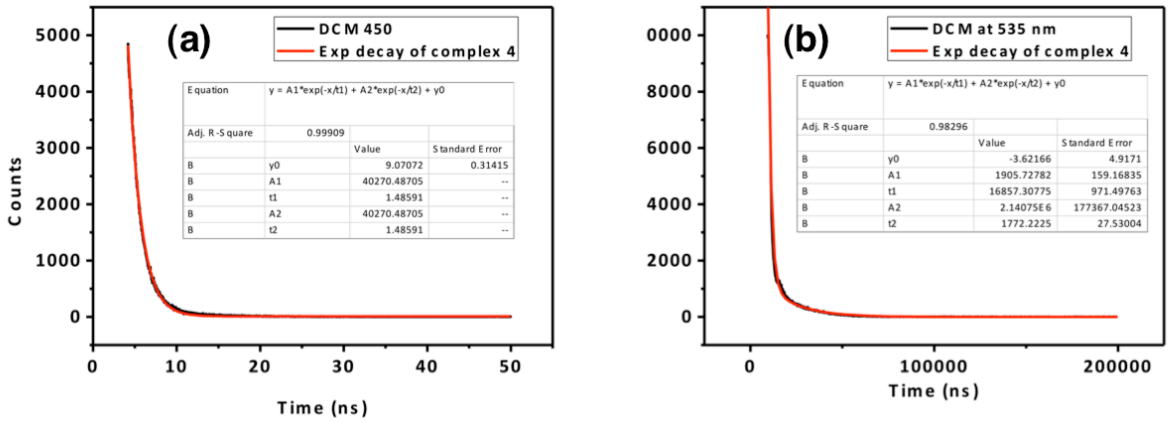

Figure S16. Emission decay profiles of **4** in DCM at different emission maxima (a) at 450 nm and (b) at 535 nm.

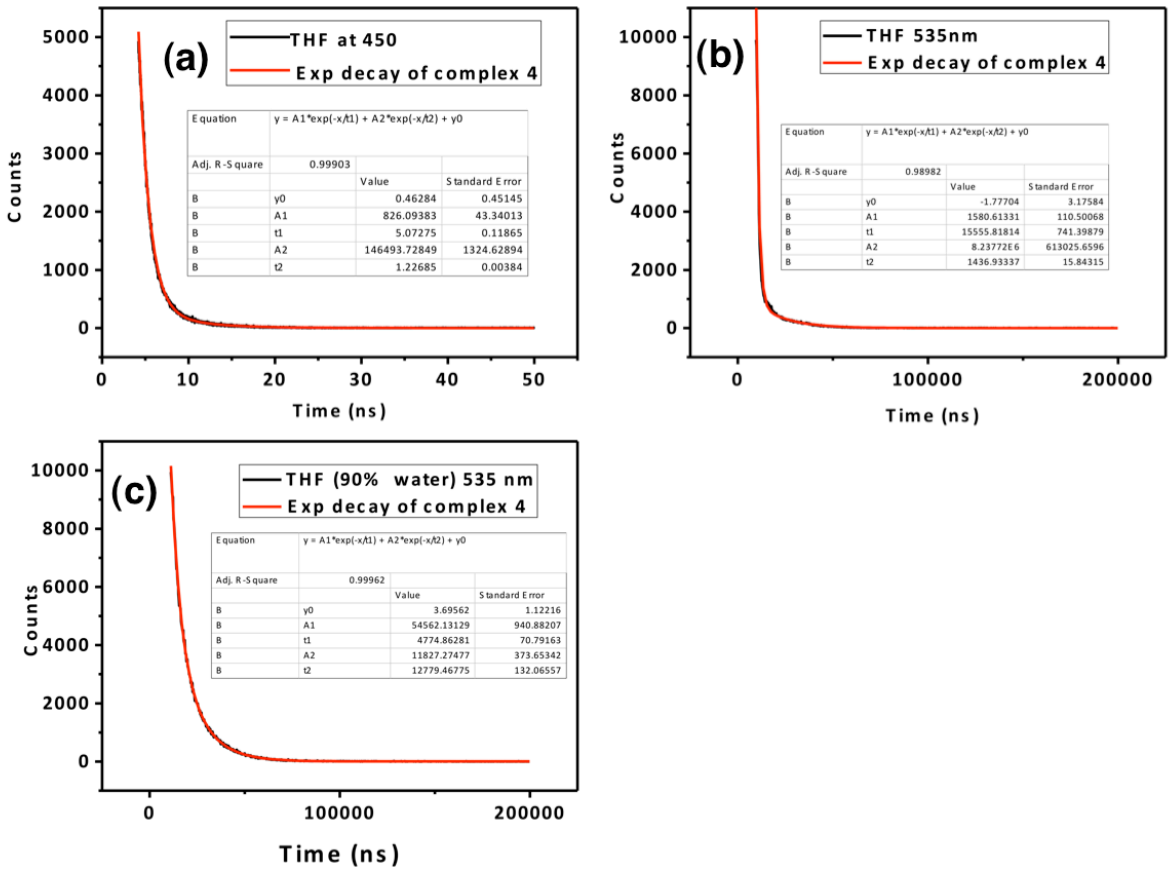

Figure S17. Emission decay profiles of **4** in THF at different emission maxima (a) at 450 nm and (b) at 535 nm at fw=0% and (c) at 535 nm at fw=90%.

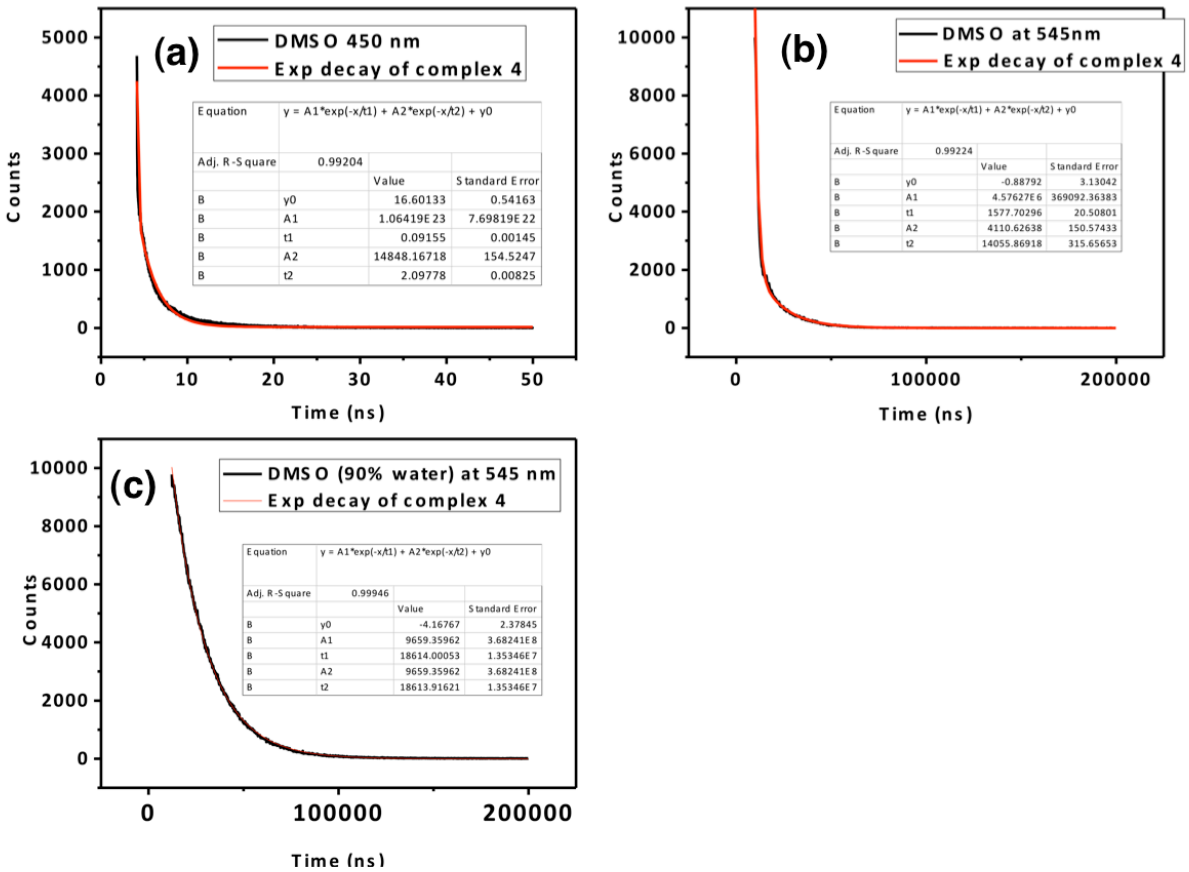

Figure S18. Emission decay profiles of **4** in DMSO at different emission maxima maxima (a) at 450 nm and (b) at 535 nm at fw=0% and (c) at 535 nm at fw=90%.

Table S1. Lifetime measurement data in different solvents

Solvent	Life time (ns) at 430 nm emission	Life time (μs) at 535 nm emission in 0% water	Life time (μs) at 535 nm emission in 90% water
DMSO	0.091	1.59	18.3
Benzene	1.21	1.59	
THF	1.24	1.44	6.2
DCM	1.4	1.78	

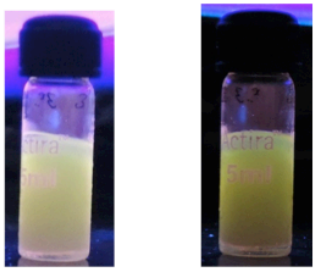

(a) (b)

Figure S19. Photographs of the emission of **4** in (a) benzene and (b) 1,4-dioxane at -80ºC under excitation at 365 nm.

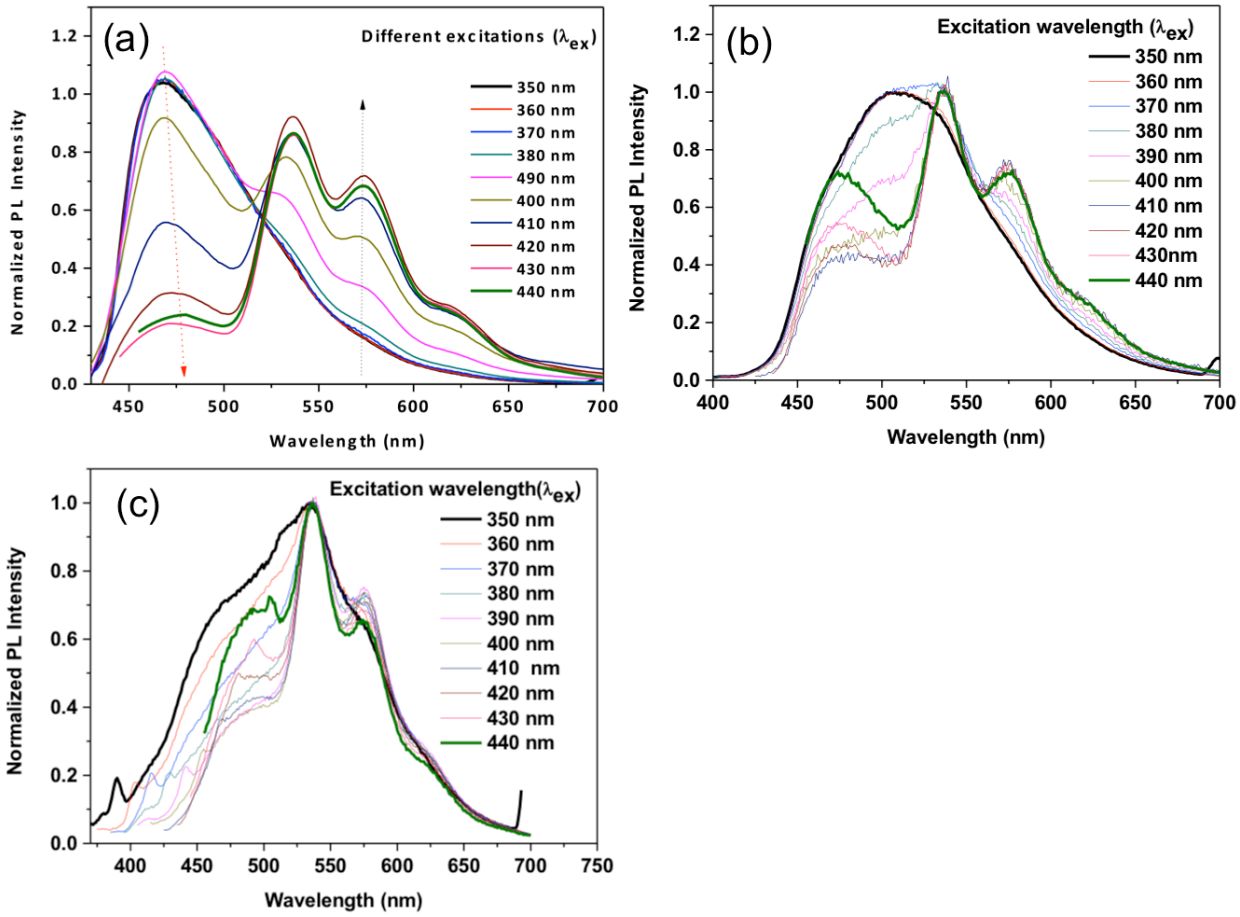

Figure S20. Excitation dependent emission spectra of complex **4** in different solvents (a) Benzene, (b) DCM and (c) DMSO; [C=1x10^{-5}M].

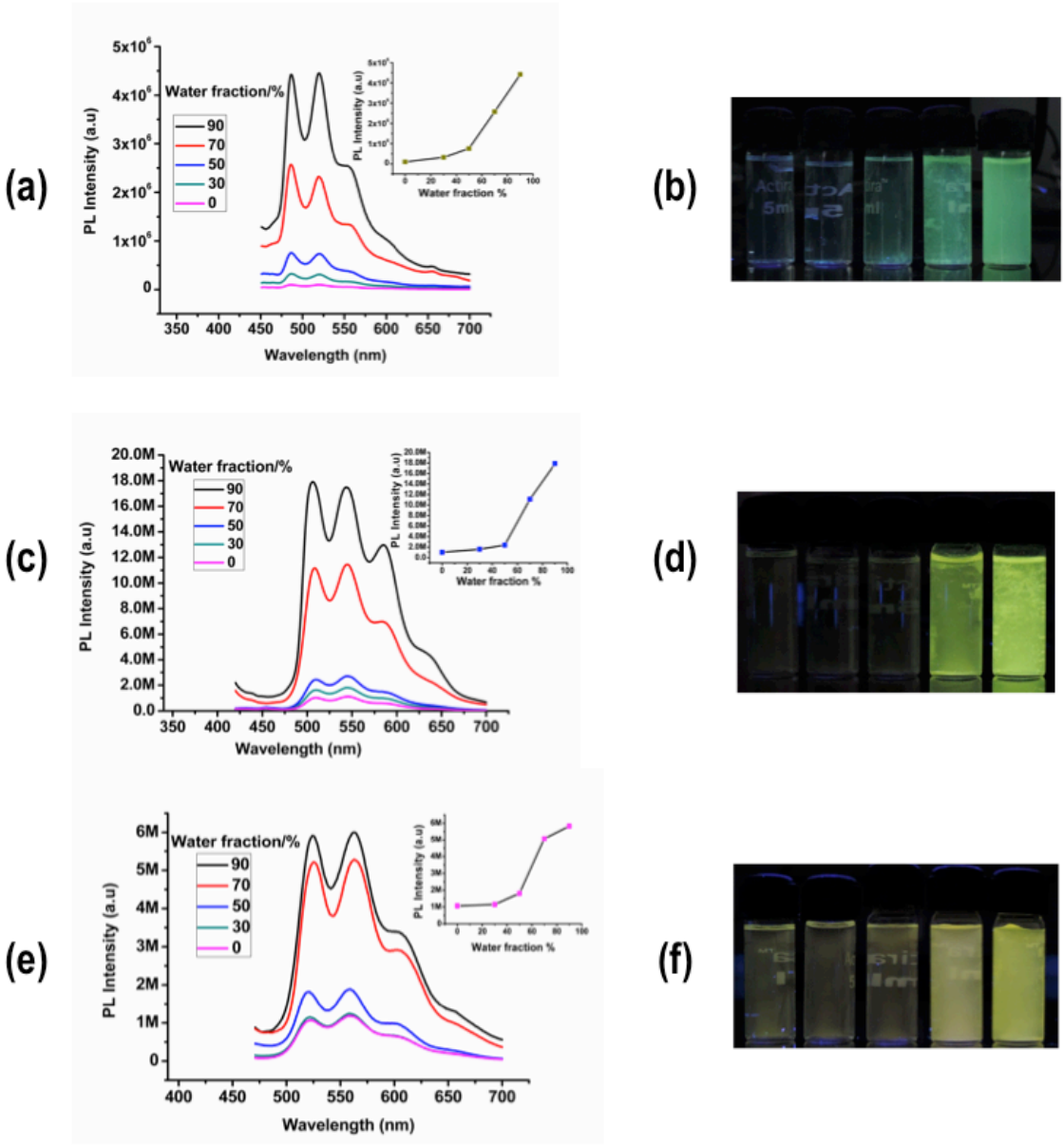

Figure S21. Emission spectra of **1**-**3** (a, c and e) in THF/water mixtures (0-90%) [inset: plot of PL intensity versus the composition of the aqueous mixtures], concentration: $1x10^{-5}$ M. Photographs of **1**-**3** (b, d and f) in THF/water taken under UV illumination (excitation: 365 nm).

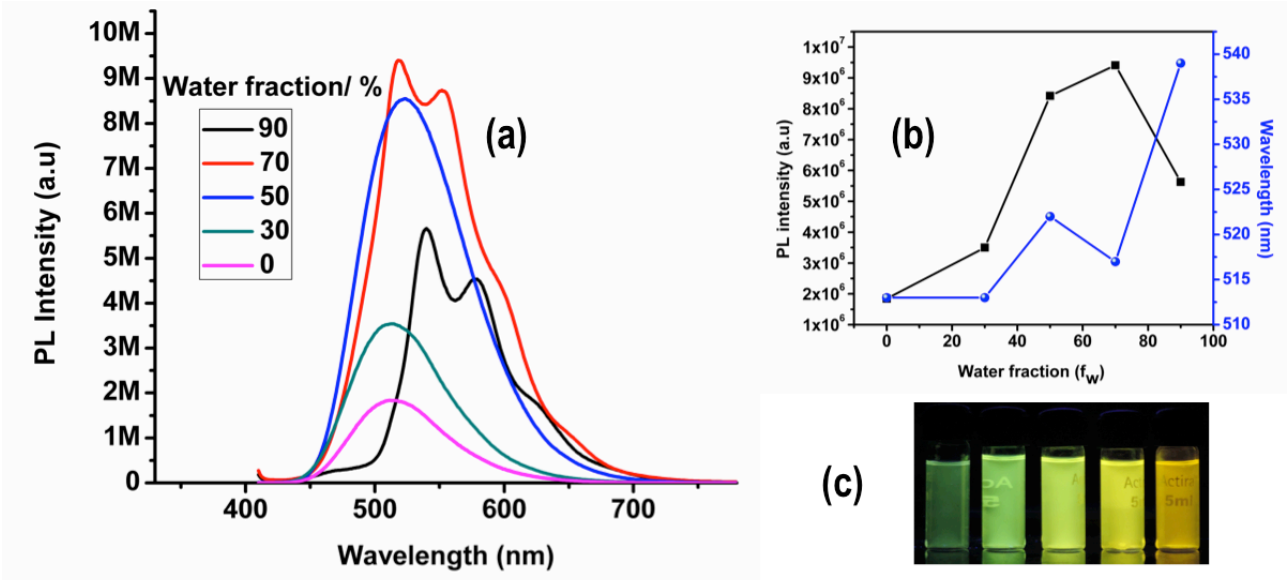

Figure S22. (a) Emission spectra of **4** in ACN/water mixtures (0-90%). (b) Plot of maximum emission intensity and wavelength (λ_{max}) of **4** versus water fraction. Concentration of **4**: $1x10^{-5}$ M. (c) Photographs of **4** in ACN/ water mixtures taken under UV illumination.

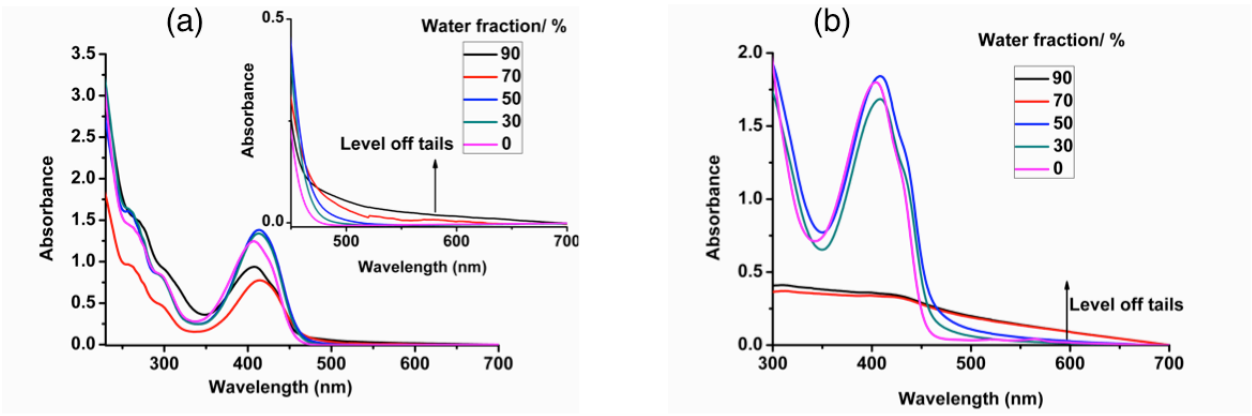

Figure S23. Absorption spectra of **4** in (a) ACN and (b) DMSO with different water fractions.

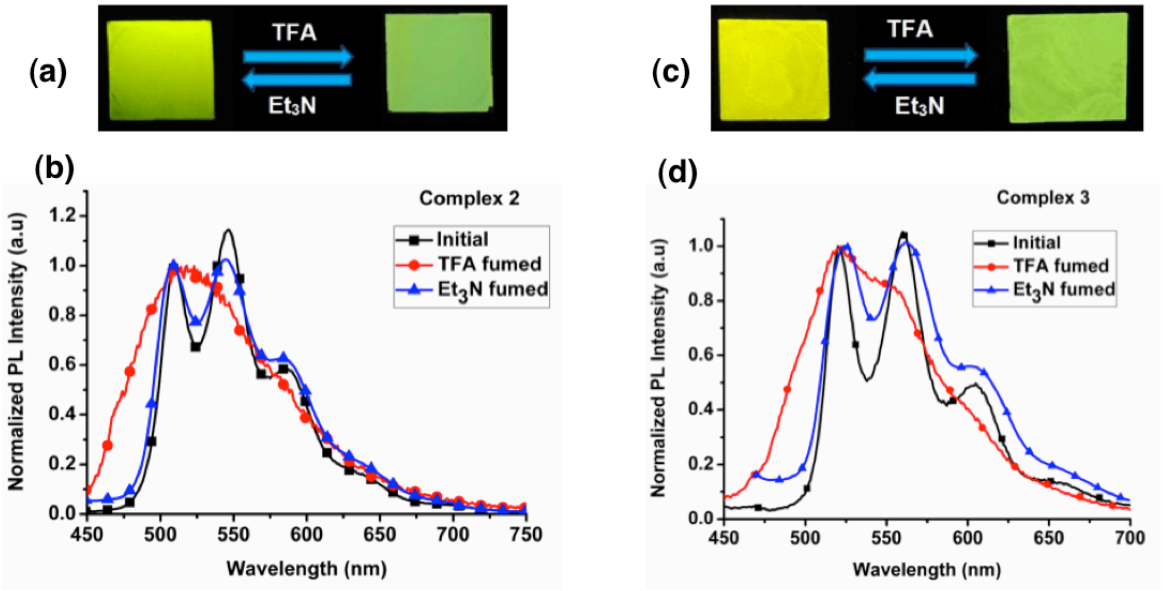

Figure S24. Thin film reversal of emission color upon TFA/Et_3N exposure and emission spectra of complexes **2** (a and b) and **3** (c and d). The photographs were taken under a wavelength excitation of 365 nm .

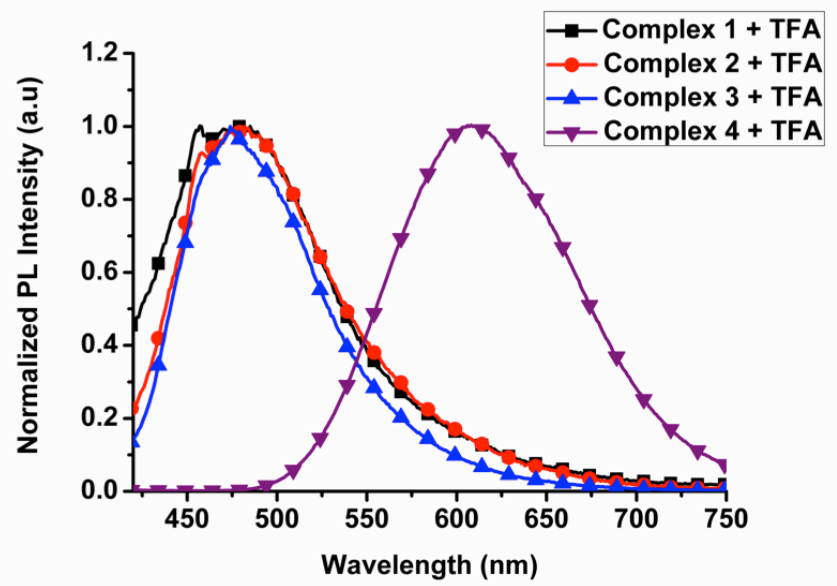

Figure S25. Emission spectra of **1-4** in DCM in presence of TFA.

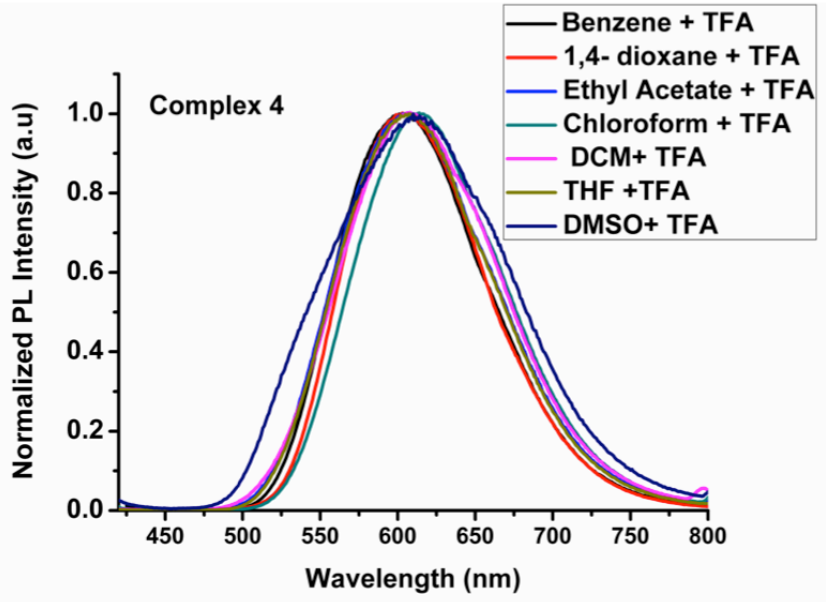

Figure S26. Emission spectra of **4** in different solvents + TFA.

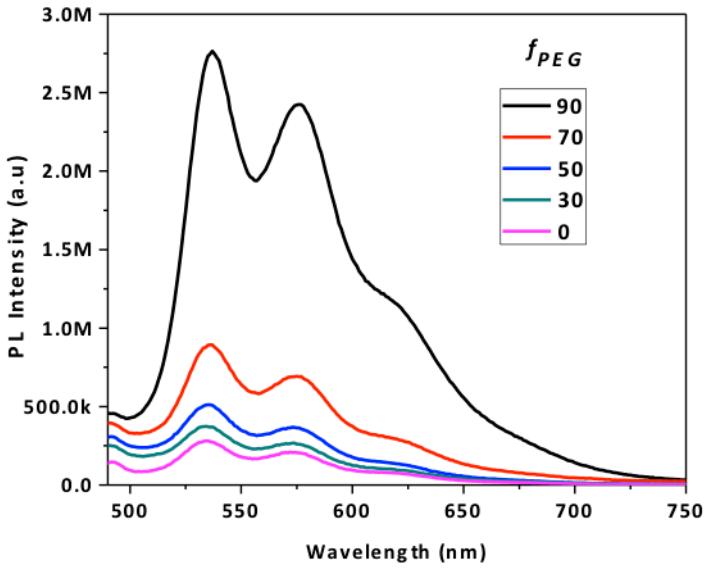

Figure S27. Emission spectra of complex **4** in PEG-THF mixture with [C = $1x10^{-5}$M, λ ex = 410 nm]. PEG = polyethylene glycol.

Section 3. Theory and Computation

Molecular geometries

In both structures, the crystal monomer and the optimized singlet ground state, the angles between trans ligands are very similar and in the range of 170-180º. The largest differences arise in the Ir-C, Ir-N and Ir-Cl bond lengths, which are overestimated by ~0.05-0.09 Å in the optimized geometries. Intermolecular effects in the crystal could be responsible for the difference in the Ir-Cl bond length but don't seem to be responsible for the differences in the Ir-C and Ir-N bond lengths, thus, we attribute these to the inherent approximations of the computational methodology. Superposition of both structures reveals that the phosphine ligands are practically identical in both geometries. Comparison of the two phosphine ligands in the complex reveals that they are enantiomers, with the iridium's equatorial plane acting as the mirror plane (Figure S20).

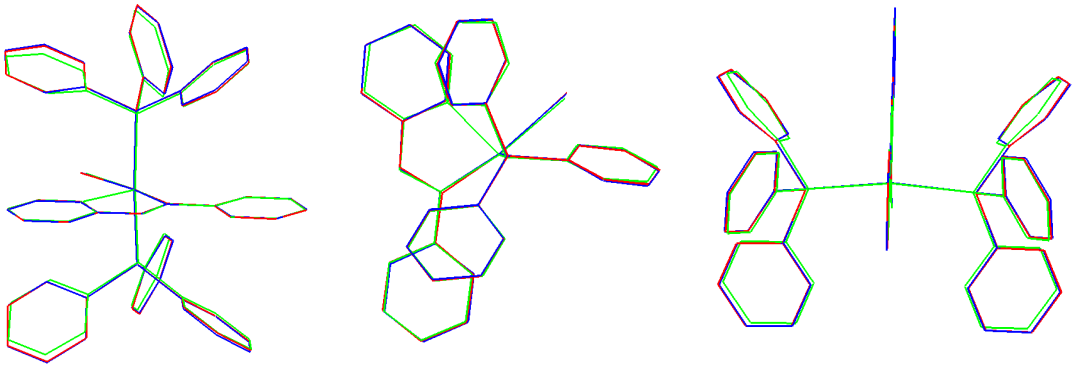

Figure S28. Different views of the superposition of the crystal's monomer (green) of complex **2** with the optimized ground state (blue) and lowest triplet state (red) at the B3LYP/LANL2DZ,6-31G(d) level. Hydrogen atoms have been omitted for the sake of clarity.

Table S2. Selected geometrical parameters of the iridium's coordination environment and the imine group (C-N, N=C and C-C) in the crystal (x-ray structure) and for the S_0 and T_1 states of complex **2** optimized at the B3LYP/LANL2DZ,6-31G(d) level.

	bond lengths (Å)								angles (º)		
	Ir-C	Ir-Cl	Ir-N	Ir-H	Ir-P	C-N	N=C	C-C	C-Ir-Cl	N-Ir-H	P-Ir-P
crystal	1.983	2.476	2.101	1.582	2.325	1.485	1.313	1.483	172	180	169
S_0	2.021	2.561	2.176	1.601	2.400	1.373	1.323	1.494	171	174	169
T_1	2.024	2.558	2.164	1.602	2.405	1.314	1.425	1.425	172	175	169

Molecular orbitals

From the HOMO to HOMO-7 (Figure S29), there are only two orbitals that do not have participation of the iridium atom. That is, HOMO-3 which is a combination of the non-bonding orbital of the nitrogen atom of the imine unit with the p_x orbital of the chloride ligand, and HOMO-5 which is a π-orbital of the phenyl ring of the Schiff base ligand. LUMO+1 is mainly a d_{z^2} type orbital with some participation of π-type orbitals of the phenyl rings of the phosphines and lies ~0.6 eV above the LUMO due to the anti-bonding interaction with the lone pair of the phosphorous. The $d_{x^2-y^2}$ type orbital on the other hand, appears rather high in energy due to strong anti-bonding interactions with orbitals of the hydride ligand, the phosphorus atoms and the nitrogen of the Schiff base.

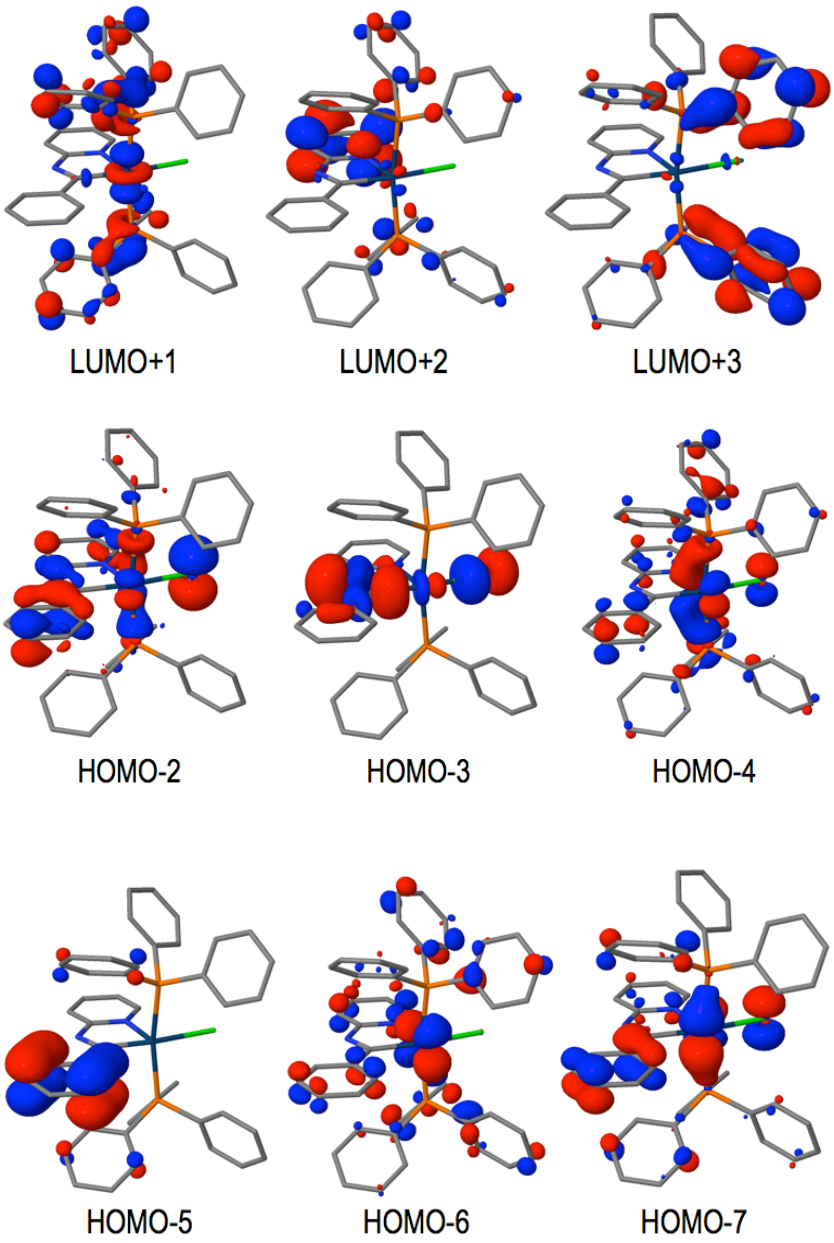

Figure S29. Selected molecular orbital plots of **2** computed at the B3LYP/LANL2DZ,6-31G(d) level

Table S3. Data relative to the most intense electronic transitions of the simulated absorption spectra of **2** computed at the B3LYP/LANL2DZ,6-31G(d) level.

State	ΔE / eV	λ / nm	f	Contributions	Assignment[1]
S_2	3.37	368	0.04	H-1→L (89%)	$ML_{Cl}L_{SB}CT/L_{SB}C$
S_4	3.74	332	0.03	H-2→L (20%)	$ML_{Cl}L_{SB}CT/L_{SB}C$
				H→L+1 (61%)	$d\text{-}d/ML_{Cl}L_{Ph}CT/L_{Cl}MCT$
S_5	3.80	326	0.11	H-2→L (58%)	$ML_{Cl}L_{SB}CT/L_{SB}C$
				H→L+1 (27%)	$d\text{-}d/ML_{Cl}L_{Ph}CT/L_{Cl}MCT$
S_7	4.04	307	0.11	H-4→L (77%)	$ML_{Cl}L_{SB}CT$
S_{12}	4.29	289	0.09	H-2→L+1 (63%)	$d\text{-}d/ML_{Cl}L_{SB}L_{Ph}CT/L_{Cl}L_{SB}MCT$
				H-1→L+3 (22%)	$ML_{Cl}L_{SB}L_{Ph}CT$
S_{13}	4.34	286	0.05	H-2→L+1 (23%)	$d\text{-}d/ML_{Cl}L_{SB}L_{Ph}CT/L_{Cl}L_{SB}MCT$
				H-1→L+3 (56%)	$ML_{Cl}L_{SB}L_{Ph}CT$
S_{15}	4.35	285	0.05	H-7→L (33%)	$ML_{Cl}L_{SB}CT/L_{SB}C$
				H-6→L (28%)	$ML_{SB}CT$
				H-1→L+2 (16%)	$ML_{Cl}L_{SB}CT/L_{SB}C$
S_{47}	4.90	253	0.12	H-7→L+1 (24%)	$d\text{-}d/ML_{Cl}L_{SB}L_{Ph}CT/L_{Cl}L_{SB}MCT$
				H-6→L+1 (16%)	d-d
				H-4→L+1 (18%)	$d\text{-}d/ML_{Cl}L_{Ph}CT/L_{Cl}MCT$
S_{48}	4.92	252	0.09	H-4→L+2 (70%)	$ML_{Cl}L_{SB}CT$

[1]Key:

$LC = \pi_L \rightarrow \pi_L^*$; $L_iLCT = L_i \rightarrow L$; $d\text{-}d = d_{ij} \rightarrow dz^2$ (i,j=x,y,z)

$MLCT = d_{ij} \rightarrow \pi_L$; $LMCT = \pi_L \rightarrow d_{ij}$ (i,j=x,y,z)

$ML_1LCT = MLCT + L_1LCT$; $ML_1L_2LCT = MLCT + L_1LCT + L_2LCT$

$L_1L_2MCT = L_1MCT + L_2MCT$

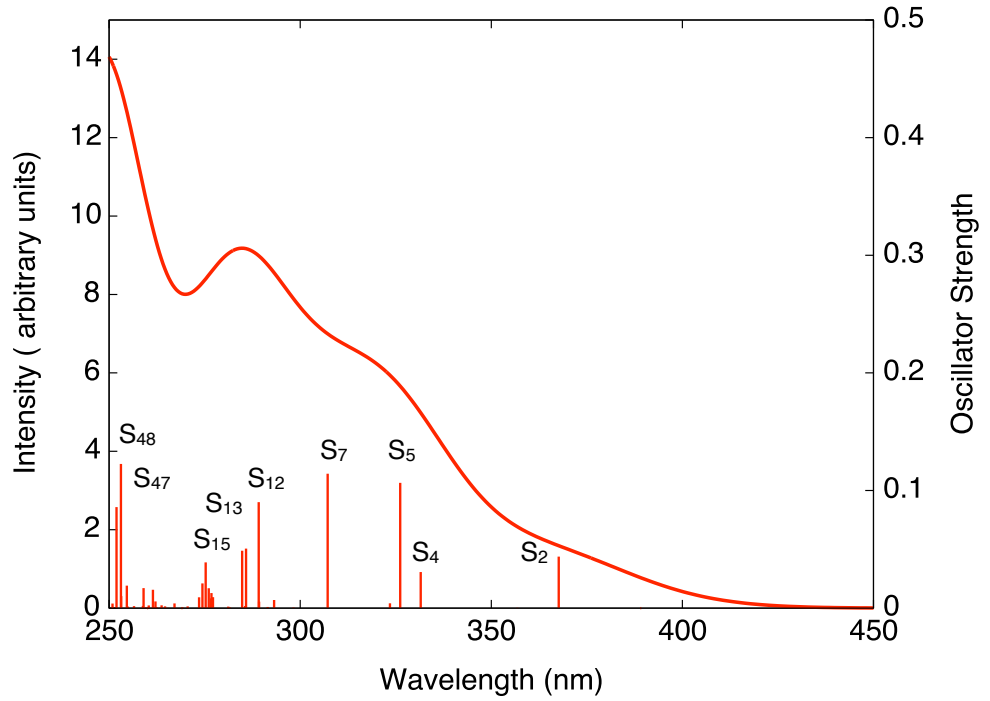

Figure S30. Simulated absorption spectra of **2** along with stick spectra computed at the B3LYP/LANL2DZ,6-31G(d) level.

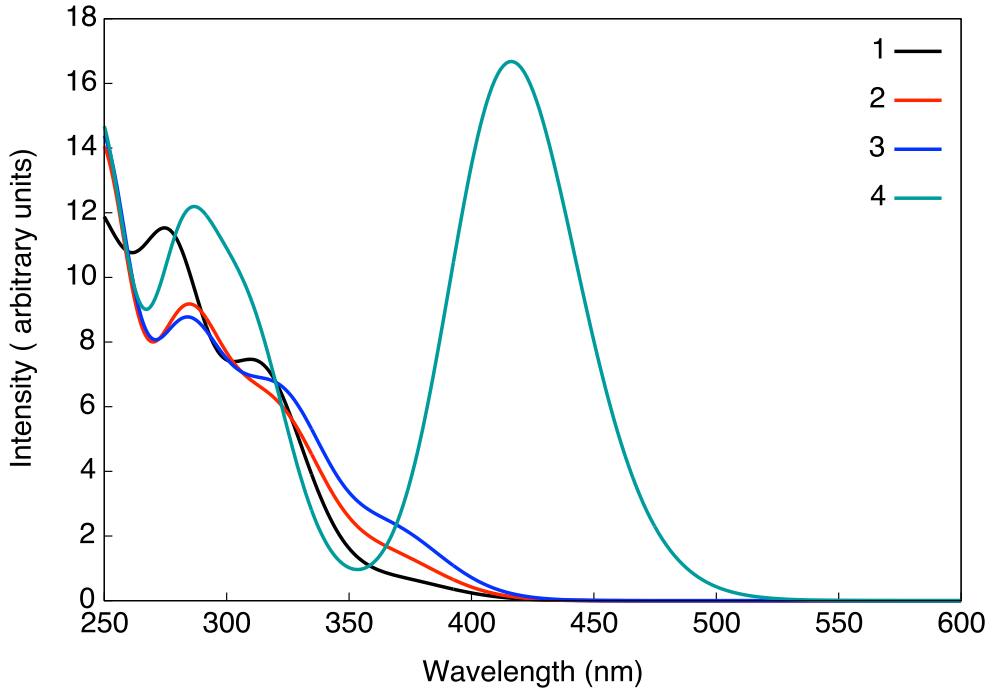

Figure S31. Simulated absorption spectra for complexes **1-4** computed at the B3LYP/LANL2DZ,6-31G(d) level.

Table S4. Calculated x,y color coordinates for complexes **1-4**.

(x,y)	1	2	3	4
solution	(0.29, 0.53)	(0.36, 0.59)	(0.40, 0.56)	(0.44, 0.50)
thin film	-	(0.36, 0.59)	-	-

Emission spectra of 1-3

Our calculations predict the ^{3}MLLCTz/LC state as the one responsible for the phosphorescence emission of complexes **1-3**. For all three complexes there is a nice agreement between experimental emission spectra and the simulated vibrationally resolved phosphorescence profiles (Figures 6, S32 and S33). Each spectrum has clearly three peaks at the short wavelength region and several less intense shoulders at long wavelengths. The relative positions of the well-resolved peaks in the emission band are correctly reproduced by our calculations, but the relative intensities are, in some cases, not correctly estimated, especially for the peak just above 500 nm. Although the peak at ~550 nm is also the most intense in our calculations, the relative intensities with the two neighboring peaks are over and underestimated, respectively. The blue shift of the 0-0 transition with respect to the convoluted peak at ~500 nm is due to the presence of nearby transitions which contribute to the band's intensity.

For complexes **1-3**, the main vibrational mode responsible for the structured emission is related to the stretching of the C=N bond in the Schiff base, with a computed frequency of ~1470-1450 cm^{-1} (Figure S34). The distortion associated with this mode is in fact the main geometrical modification along the molecular relaxation on the T_1 state potential energy surface from the Franck-Condon region. Although this vibrational progression is the one that apparently causes the overall shape of the emission spectra, there are also other normal modes contributing to the emission profiles (Tables S5-S8). Apart from the C=N vibronic progression, there are combinations of modes of the iminie unit with modes involving the phenyl rings of the PPh_3 ligands. Since the modifications in the ancillary ligand of complexes **1-3** do not have a great impact on the C=N stretching mode, the peaks of the vibrational progressions in the emission spectra are similarly spaced out in the three complexes and the relative intensities are alike. The main effect of the substitution is therefore in tuning the energy of the electronic transition from the T_1 state back to the ground state, and not in the modification of the overall shape of the emission spectrum.

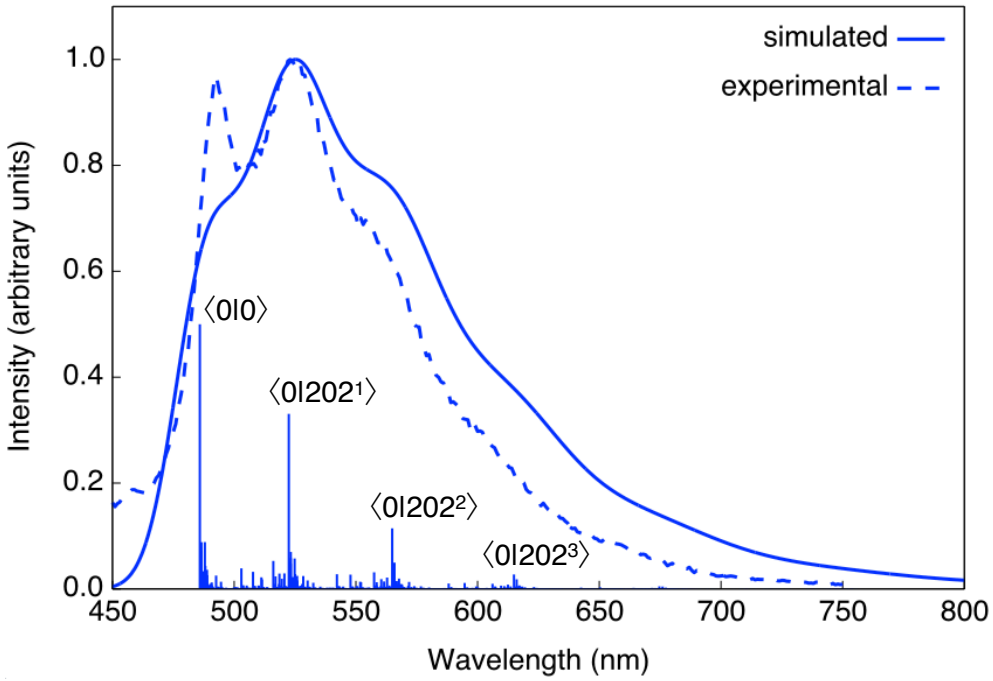

Figure S32. Simulated (solid) and experimental (dashed) emission spectra of complex **1** together with the calculated stick spectrum obtained at the B3LYP/LANL2DZ,6-31G(d) computational level. Both spectra have been normalized and the calculated spectrum has been blue shifted by 0.09 eV to superimpose the most intense peaks. The 202 normal mode of vibration corresponds to the C=N stretching mode of the imine.

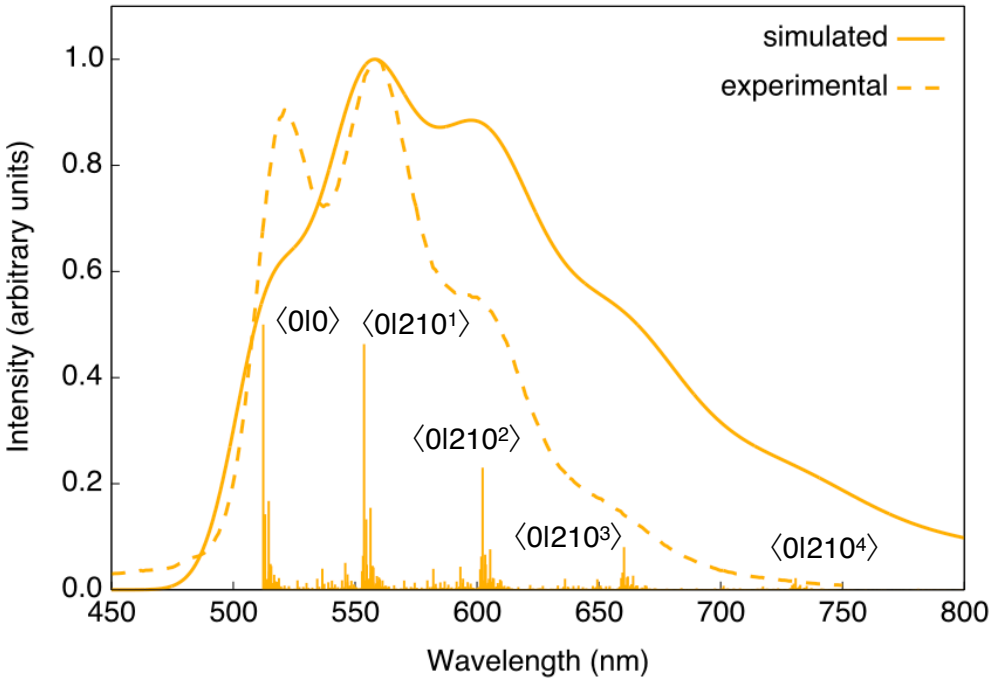

Figure S33. Simulated (solid) and experimental (dashed) emission spectra of complex **3** together with the calculated stick spectrum obtained at the B3LYP/LANL2DZ,6-31G(d) computational level. Both spectra have been normalized and the calculated spectrum has

been blue shifted by 0.12 eV to superimpose the most intense peaks. The 210 normal mode of vibration corresponds to the C=N stretching mode of the imine.

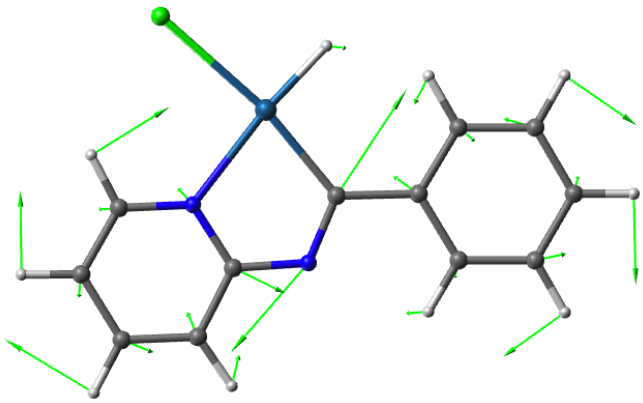

Figure S34. Displacement vectors of the normal mode responsible for the vibronic progressions observed in the emission spectra of complex **2**. The triphenylphosphine ligands have been omitted for greater clarity.

Table S5. Energy, wavelength, intensity (arbitrary units) and assignation of the most intense transitions of the calculated stick spectra of complex **1**, blue-shifted by 0.09 eV.

λ / nm	ΔE / eV	Intensity	Assignation
486	2.55	0.50	**⟨0|0⟩**
486	2.55	0.08	$\langle 0|2^1\rangle$
487	2.55	0.09	$\langle 0|5^1\rangle$
487	2.55	0.07	$\langle 0|6^1\rangle$
488	2.54	0.09	$\langle 0|20^1\rangle$
516	2.40	0.05	$\langle 0|177^1\rangle$
522	2.37	0.33	**$\langle 0|202^1\rangle$**
565	2.19	0.11	**$\langle 0|202^2\rangle$**
523	2.37	0.07	$\langle 0|203^1\rangle$
523	2.37	0.05	$\langle 0|202^1;2^1\rangle$
523	2.37	0.06	$\langle 0|202^1;5^1\rangle$
525	2.36	0.06	$\langle 0|202^1;20^1\rangle$

Table S6. Energy, wavelength, intensity (arbitrary units) and assignation of the most intense transitions of the calculated stick spectra of complex **2**, blue-shifted by 0.12 eV.

λ / nm	ΔE / eV	Intensity	Assignation
503	2.46	0.49	**<0|0>**
503	2.46	0.09	$\langle 0|5^1\rangle$
503	2.46	0.07	$\langle 0|6^1\rangle$
505	2.46	0.10	$\langle 0|20^1\rangle$
535	2.32	0.05	$\langle 0|179^1\rangle$
542	2.29	0.50	**$\langle 0|204^1\rangle$**
589	2.11	0.28	**$\langle 0|204^2\rangle$**
643	1.93	0.11	**$\langle 0|204^3\rangle$**
544	2.28	0.05	$\langle 0|212^1\rangle$
543	2.28	0.10	$\langle 0|204^1;5^1\rangle$
590	2.10	0.05	$\langle 0|204^2;5^1\rangle$
543	2.28	0.08	$\langle 0|204^1;6^1\rangle$
545	2.28	0.10	$\langle 0|204^1;20^1\rangle$
592	2.10	0.06	$\langle 0|204^2;20^1\rangle$
590	2.10	0.06	$\langle 0|212^1;204^1$

Table S7. Energy, wavelength, intensity (arbitrary units) and assignation of the most intense transitions of the calculated stick spectra of complex **3**, blue-shifted by 0.12 eV.

λ / nm	ΔE / eV	Intensity	Assignation
512	2.42	0.50	**<0|0>**
513	2.42	0.14	<0|6^1>
515	2.41	0.17	<0|21^1>
546	2.27	0.05	<0|182^1>
553	2.24	0.06	<0|209^1>
554	2.24	0.46	**<0|210^1>**
602	2.06	0.23	**<0|210^2>**
660	1.88	0.08	**<0|210^3>**
555	2.24	0.13	<0|210^1;6^1>
603	2.05	0.07	<0|210^2;6^1>
556	2.23	0.15	<0|210^1;21^1>
605	2.05	0.08	<0|210^2;21^1>
602	2.06	0.06	<0|210^1;209^1

Table S8. Vibration normal modes that contribute to the simulated emission spectra together with their frequency and nature.

Complex	NMV	Frequency / cm^{-1}	Assignation
1	2	20.2	PPh_3
	5	28.1	PPh_3
	6	28.7	PPh_3
	20	87.5	PPh_3
	177	1203.9	C_{Ph}-C_{Ir}
	202	1439.8	C_{Ir}=N
	203	1468.9	C_{Ir}=N
2	5	28.5	PPh_3
	6	29.0	PPh_3
	20	86.7	PPh_3
	179	1203.7	C_{Ph}-C_{Ir}
	204	1450.5	C_{Ir}=N
	212	1494.1	C_{Ir}=N
3	6	28.2	PPh_3
	21	84.8	PPh_3
	182	1203.5	C_{Ph}-C_{Ir}
	209	1444.4	C_{Ir}=N & CH_3
	210	1458.9	C_{Ir}=N & CH_3

Torsion of the Schiff base ligand in complex 4

To further explore the nature of the lowest spin singlet electronic transition in complex **4**, which corresponds to the intra-ligand charge transfer singlet state (^{1}ILCT) localized on the Schiff base ligand, we compute its energy profile in benzene and DMSO along the molecular torsion of the diphenylamine donor group in the Schiff base ligand (Figure S35).

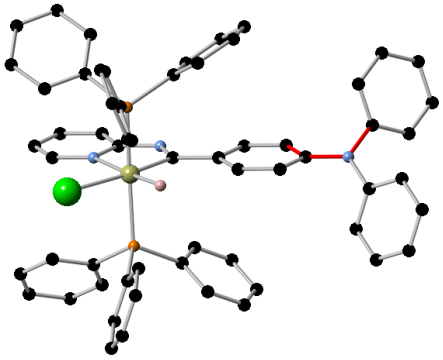

Figure S35. Molecular torsion in the Schiff base ligand of complex **4**.

Our results (Figure S36) indicate that the potential energy minimum of ^{1}ILCT corresponds to the same dihedral angle between the phenyl rings of the donor group and the planar Schiff base ligand obtained for the optimized ground state. Moreover, this picture is virtually the same for the two explored solvents. These results force us to rule out the formation of a twisted intramolecular charge transfer (TICT) state.

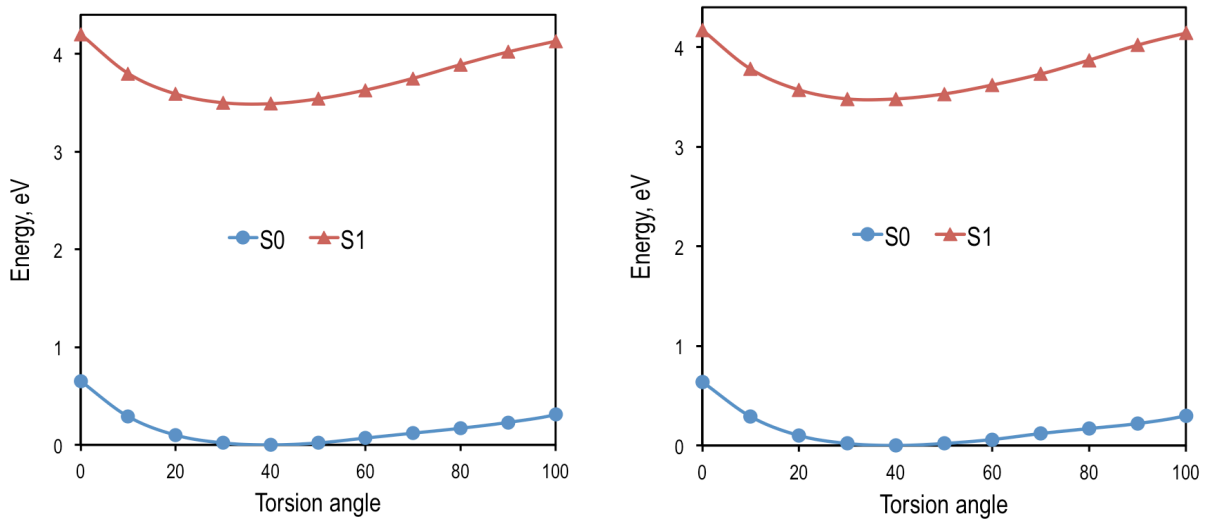

Figure S36. Energy profiles of the ground (S_0) and ^{1}ILCT (S_1) states of complex **4** along the molecular torsion in benzene (left) and DMSO (right) computed at the CAM-B3LYP level.

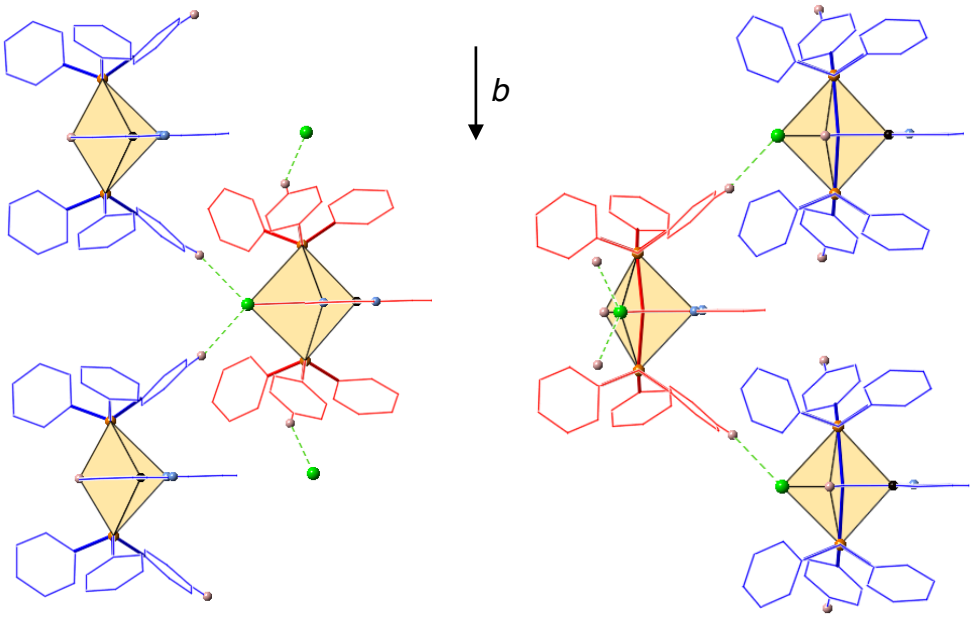

Figure S37. Side view of the C-H···Cl interactions of **2** shown in Figure 11 between a complex in the reference chain (red) and complexes of the blue chains.

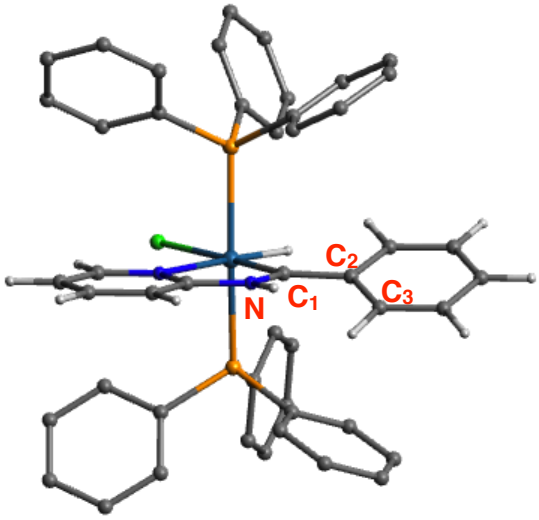

Figure S38. Optimized S_0 geometry of **2H**. Hydrogen atoms of the PPh_3 ligands are omitted for the sake of clarity.

Table S9. Relative energies (in kcal/mol) of different protonated forms of complexes **1** and **4** (Scheme S1).

	Protonated site	
complex	N2	N3
1	0.0	12.3
4	0.0	35.2

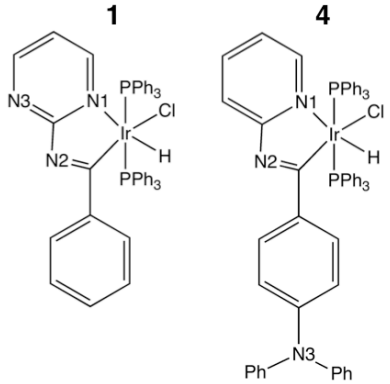

Scheme S1. Complexes **1** and **4** with labels of N atoms corresponding to Table S8 protonated sites.

Table S10. Selected geometrical parameters of the iridium's coordination environment and of the imine group (C-N, N=C and C-C) for the optimized S_0 and T_1 states of **2H**. In Δ, the difference of the optimized S_0 geometrical parameters of **2H** relative to the original optimized S_0 of **2** are shown. The δ dihedral angle corresponds to the $N=C_1-C_2-C_3$ shown in Figure S38.

geometry	bond lengths (Å)							
	Ir-C	Ir-Cl	Ir-N	Ir-H	Ir-P	C-N	N=C	C-C
S_0	1.965	2.491	2.213	1.585	2.443	1.397	1.362	1.474
T_1	2.064	2.401	2.188	1.588	2.459	1.357	1.394	1.439
Δ	-0.056	-0.070	0.037	-0.016	0.043	0.024	0.039	-0.020

geometry	angles (º)			
	C-Ir-Cl	N-Ir-H	P-Ir-P	δ
S_0	176	174	168	22
T_1	163	157	175	21
Δ	5	-1	-0	22

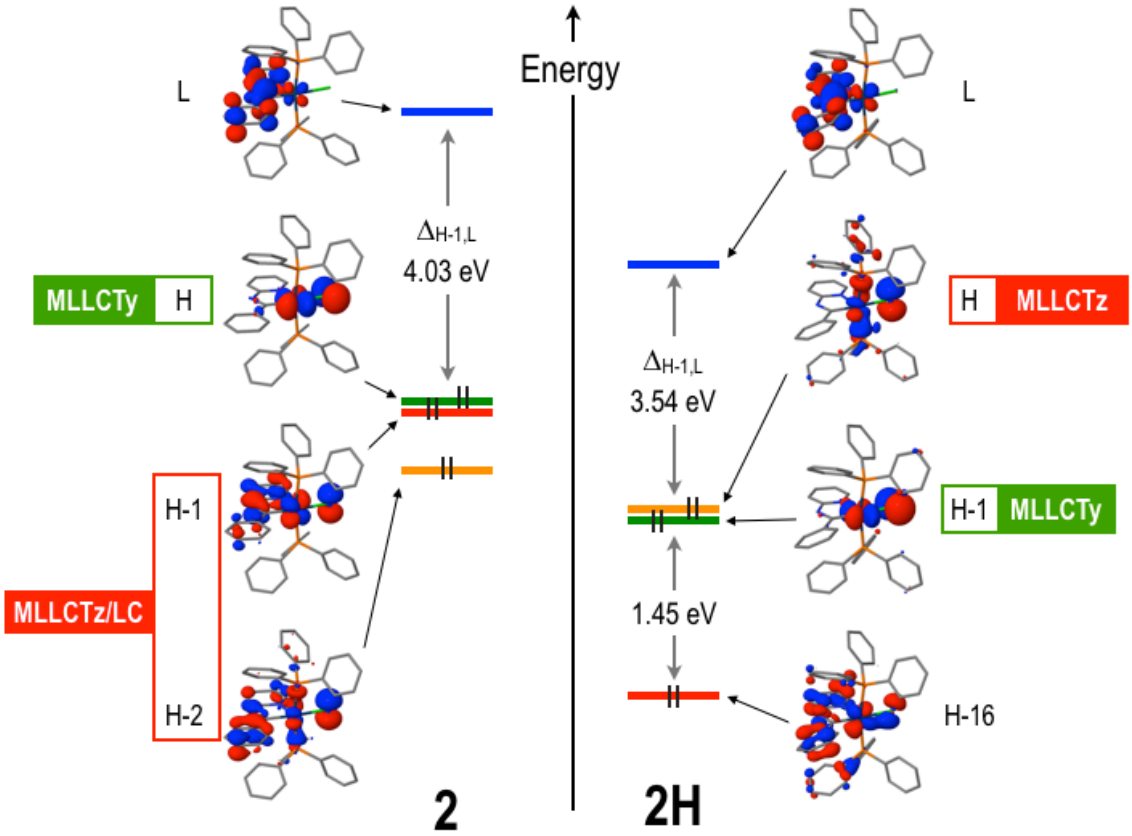

Figure S39. Representation of the molecular orbital diagram of complex **2** in its neutral (left) and protonated (right) forms. MLLCTz and MLLCTy labels indicate occupied MOs contributing to the corresponding lowest lying triplet states. Note: distribution of the MOs along the vertical axis only corresponds to a qualitative schematic representation of their relative energy.

Table S11. Excitation energies (in eV) to the two lowest lying triplet states of complex **2** and its protonated form (**2H**).

Complex **2**		Complex **2H**	
Character	Energy	Character	Energy
MLLCTz/LC	2.63	MLLCTz	2.69
MLLCTy	3.12	MLLCTy	2.61

Table S12. HOMO and LUMO energies (in eV) of complex **4** computed with CAM-B3LYP in benzene and DMSO solution. Δ indicates *E*(DMSO) – *E*(benzene).

Character	Benzene	DMSO	Δ
LUMO	-0.70	-0.92	-0.12
HOMO	-6.04	-6.19	-0.08